

An Asymptotically Compatible Formulation for Local-to-Nonlocal Coupling Problems without Overlapping Regions

Huaiqian You^a, Yue Yu^a, David Kamensky^b

^aDepartment of Mathematics, Lehigh University, Bethlehem, PA 18015, USA

^bDepartment of Mechanical and Aerospace Engineering, The University of California, San Diego, CA, 92093

Abstract

In this paper we design and analyze an explicit partitioned procedure for a 2D dynamic local-to-nonlocal (LtN) coupling problem, based on a new nonlocal Robin-type transmission condition. The nonlocal subproblem is modeled by the nonlocal heat equation with a finite horizon parameter δ characterizing the range of nonlocal interactions, and the local subproblem is described by the classical heat equation. We consider a heterogeneous system where the local and nonlocal subproblems present different physical properties, and employ no overlapping region between the two subdomains. We first propose a new generalization of classical local Neumann-type condition by converting the local flux to a correction term in the nonlocal model, and show that the proposed Neumann-type boundary formulation recovers the local case as $O(\delta^2)$ in the L^∞ norm. We then extend the nonlocal Neumann-type boundary condition to a Robin-type boundary condition, and develop a local-to-nonlocal coupling formulation with Robin-Dirichlet transmission conditions. To stabilize the explicit coupling procedure and to achieve asymptotic compatibility, the choice of the coefficient in the Robin condition is obtained via amplification factor analysis for the discretized system with coarse grids. Employing a high-order meshfree discretization method in the nonlocal solver and a linear finite element method in the local solver, the selection of optimal Robin coefficients are verified with numerical experiments on heterogeneous and complicated domains. With the developed optimal coupling strategy, we numerically demonstrate the coupling framework's asymptotic convergence to the local limit with an $O(\delta) = O(h)$ rate, when there is a fixed ratio between the horizon size δ and the spatial discretization size h .

Keywords: nonlocal heat equation, asymptotic compatibility, Robin condition, explicit coupling strategy, heterogeneous system

Contents

1	Introduction	2
2	Preliminaries on Local and Nonlocal Models	5
2.1	Nonlocal Heat Problem	6

Email address: yuy214@lehigh.edu (Yue Yu)

2.2	Local Heat Problem	8
3	Boundary Conditions for Nonlocal Problems	9
3.1	A Nonlocal Neumann-Type Boundary Condition	10
3.2	A Nonlocal Robin-Type and Corner Boundary Condition	17
3.3	Numerical Results for Nonlocal Boundary Conditions	19
3.3.1	Test 1: a square domain with a straight line boundary	20
3.3.2	Test 2: a circular domain	21
3.3.3	Test 3: a cross-shape domain	22
4	Nonoverlapping Local-to-Nonlocal (LtN) Coupling Framework	24
4.1	An Explicit Coupling Approach with Robin Transmission Conditions	24
4.2	Estimates for the Optimal Robin Coefficient	27
4.3	Numerical Results for Local-to-Nonlocal Coupling Framework	28
4.3.1	LtN Test 1: coupling problem with a straight line interface	29
4.3.2	LtN Test 2: coupling problem with a circular interface	34
4.3.3	LtN Test 3: coupling problem with a cross-shape interface	37
5	Conclusion	39

1. Introduction

In the last decades, there has been an increasing interest in the simulation of nonlocal integro-differential equations (IDEs) such as nonlocal diffusion and peridynamics[1–19], since they can describe phenomena not well represented by classical Partial Differential Equations (PDEs). The nonlocal models with integral operators in space allow for the description of long-range interactions and reduce the regularity requirements on problem solutions, and therefore provide exceptional simulation fidelity for a broad spectrum of applications such as fracture mechanics, anomalous subsurface transport, phase transitions, image processing, multiscale and multiphysics systems, magnetohydrodynamics, and stochastic processes.

However, despite the nonlocal IDEs’ improved accuracy, the usability of nonlocal models could be hindered by several modeling and numerical challenges such as the unconventional prescription of nonlocal boundary conditions, the calibration of nonlocal model parameters and the expensive computational cost. Moreover, in real-world applications nonlocal effects are often concentrated only in some parts of the domain, and in the remaining parts the system can be accurately described by a PDE. Thus, local-to-nonlocal coupling strategies are required such that the resultant coupling framework can support the nonlocal model near the regions where the nonlocal interaction occurs as well as the efficient classical PDE model employed for the other parts. In recent years, many strategies have been

proposed to couple local-to-nonlocal or two nonlocal models with different nonlocality [20–39]. Just to name a few, examples include the optimal-control based coupling method [24, 27], the overlapping partitioned procedure with Robin conditions [40], the Arlequin method [22, 23], the Morphing approach [21, 28, 38], the quasi-nonlocal coupling method [26, 41], the force-based blending method [29, 42], the splice method [32], the varying horizon method [20, 31, 32, 43–47], the submodeling approach [33–35], and so on. However, most of the above local-to-nonlocal coupling approaches focus on the scenario where the local and nonlocal models are physically consistent, i.e., when the nonlocal interaction range δ shrinks, the nonlocal model converges to the local model, and there is no jump of the physical properties across the local-nonlocal interface. To the authors’ best knowledge, there is very little work on dynamic local-to-nonlocal coupling approaches for heterogeneous domains where the local and nonlocal regions present dramatically different physical properties, although those approaches are required for applications with both nonlocal effects and multiscale/multiphysics dynamics.

Therefore, we aim to develop a dynamic local-to-nonlocal coupling method based on an explicit coupling partitioned procedure with transmission conditions applied on the sharp interface, so that the method is capable of handling the physical property jumps across the interface. For concreteness, in this paper we focus on coupling the nonlocal heat equation with the classical heat equation, although the proposed technique is applicable to more general problems. The numerical approximation of this type of heterogeneous system is challenging, due to potential numerical instabilities in coupling schemes for domain-decomposition problems and the nonlocal effects involved. Specifically, the local-to-nonlocal coupling method for heterogeneous systems presents both modeling and numerical difficulties/desired properties:

- To apply the transmission condition on the nonlocal side, a nonlocal boundary condition on the sharp interface is required. However, in general nonlocal boundary conditions must be defined on a layer surrounding the domain. Therefore, new definitions of the nonlocal boundary conditions are required when only the surface data are available at the sharp local-to-nonlocal interface.
- A key feature in the discretization of nonlocal models has been the concept of *asymptotic compatibility* [48], meaning that the nonlocal discretization has to recover a corresponding local model as both the nonlocal interaction range δ and the characteristic discretization lengthscale are reduced at the same rate. To ensure that the local-to-nonlocal coupling model recovers a well-understood classical limit, it is advocated that the developed coupling framework should also preserve asymptotic compatibility.
- In explicit coupling partitioned procedures, both the local and nonlocal subproblems are solved only once per time step and do not satisfy exactly the coupling transmission conditions. As a consequence, the work exchanged between the two subproblems is not perfectly balanced and this may induce instabilities in the coupling scheme. Therefore, stabilization strategies are required to develop a robust explicit coupling method with partitioned procedure.

In this paper, we address the above three difficulties with three steps. Firstly, to resolve the modeling difficulty of defining the nonlocal transmission condition we introduce a nonlocal boundary treatment that is designed to convert the local Neumann-type boundary conditions defined on sharp surfaces into nonlocal volume constraints in the nonlocal model, and rigorously prove that this nonlocal boundary value problem recovers the desired local Neumann problem with an optimal $O(\delta^2)$ rate as the nonlocal interaction range $\delta \rightarrow 0$. Based on the nonlocal Neumann-type boundary condition, we further develop the nonlocal Robin-type boundary condition on a sharp surface. Although there are several previous attempts to tackle the conversion of surface data and nonlocal volume constraints (see, e.g., [40, 49–54]), to the authors’ best knowledge the proposed formulation has for the first time provided a Robin-type boundary condition for nonlocal problems and obtained the optimal second order asymptotic convergence to the local limit. Secondly, to ensure the asymptotic compatibility of the nonlocal solver, based on the new formulation for nonlocal boundary condition we develop an asymptotically compatible meshfree discretization method with the generalized moving least squares (GMLS) approximation framework [55, 56]. In the last part of the paper, we investigate a stabilization strategy for coupling local and nonlocal heat equations. In classical domain-decomposition problems, the Robin transmission condition, which is a linear combination of the Dirichlet and Neumann transmission conditions, has been proven to be very efficient in enhancing the coupling stability in explicit partitioned procedures (see, e.g., [57–60]). Therefore, to resolve the last difficulty we propose an explicit partitioned procedure based on the developed Robin-type boundary condition applied on the sharp local-to-nonlocal interface, improving upon the implicit partitioned procedure with overlapping regions found in the literature [40]. In the nonlocal subdomain, the proposed Robin-type transmission condition is applied on the interface and the nonlocal heat equation is discretized with the meshfree discretization method. In the local subdomain, classical Dirichlet transmission condition is applied, while the classical heat model is discretized with finite elements. To investigate the optimal coupling strategy for this partitioned coupling framework, we develop stability analysis in general geometries for predicting the values of the optimal Robin coefficients numerically.

The paper is organized as follows. We first present in Section 2 governing equations of nonlocal and local models and the discretization methods, respectively. In Section 3 a nonlocal Robin-type boundary condition based on sharp surface data is proposed: we firstly develop a nonlocal Neumann-type boundary condition and provide a consistency result for the resultant nonlocal boundary value problem in Section 3.1, then generalize the nonlocal Neumann-type boundary condition to a nonlocal Robin-type boundary condition in Section 3.2. The consistency of the proposed Robin-type boundary condition is then numerically verified in Section 3.3 where the optimal $O(\delta^2)$ convergence to the local limit is obtained. With the developed nonlocal Robin condition, the coupling procedure is detailed in Section 4. For the full partitioned algorithm presented in Section 4.1, in Section 4.2 we present stability analysis for the fully discretized problem and develop a numerical approach to approximate the optimal Robin coefficient. In Section 4.3 we then demonstrate the performance of this coupling framework and verify the optimal coefficient with convergence and patch tests. To investigate the capability of this coupling framework on more complicated scenarios, we also test

the flexibility of this method for problems with different domain settings. Section 5 summarizes our findings and discusses future research.

2. Preliminaries on Local and Nonlocal Models

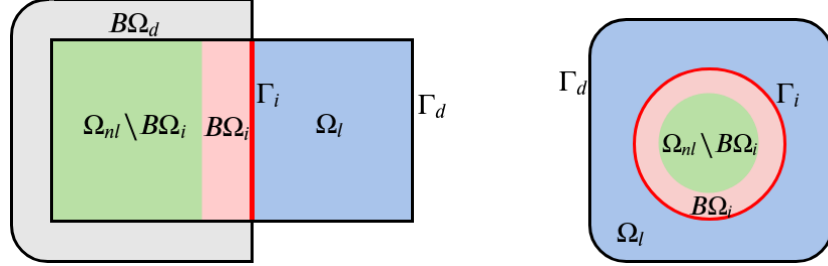


Figure 1: Notations for representative domain decomposition settings. The nonlocal subdomain Ω_{nl} is represented by the green and red regions together, local subdomain Ω_l is represented in blue, the sharp interface Γ_i is highlighted by red. Nonlocal Dirichlet boundary condition is given on $B\Omega_d$, and nonlocal Robin transmission condition is applied on the red region $B\Omega_i$. On the local subdomain, Dirichlet boundary condition is given on Γ_d and Dirichlet transmission condition is applied on Γ_i .

In this section, we define the formulation for the solution $u(\mathbf{x})$ in a two-dimensional body occupying the domain $\Omega \subset \mathbb{R}^2$. The domain Ω is composed of two parts: the nonlocal subdomain Ω_{nl} (as shown by the green and red regions in Figure 1) where the problem is described by a nonlocal model based on integro-differential equations, and the classical theory subdomain Ω_l (as shown by the blue region in Figure 1) occupied by a local model described by classical PDEs. To develop a nonoverlapping coupling framework, for both the local and nonlocal models the interface boundary conditions are applied on a 1D curve, which is marked as Γ_i . On Γ_i , a classical Dirichlet type boundary condition is applied on the local side. In the nonlocal solver, to impose a generalization of the Robin type boundary condition on Γ_i , a modified nonlocal formulation is applied in a collar region $B\Omega_i$. For the external boundary conditions, we assume that suitable Dirichlet boundary conditions are imposed on the local and nonlocal subdomains, without loss of generality. Specifically, on the external boundary of the nonlocal side, the Dirichlet boundary condition is applied on a collar consisting of all points outside the domain that interact with points inside the domain, which is marked by $B\Omega_d$ (as shown in grey in the left plot of Figure 1). On the external boundary of the local side, the Dirichlet boundary condition is applied on a sharp 1D curve Γ_d .

Although the proposed technique is applicable to more general problems, in the local subdomain Ω_l we model the problem with a classical heat equation. In the nonlocal subdomain Ω_{nl} we consider a nonlocal integro-differential equation (IDE) which is a nonlocal analog to the classical heat equation. We also assume that Γ_i and Ω_{nl} are both bounded and connected. Note that since the local and nonlocal regions interact on a sharp interface Γ_i , the proposed coupling framework can be applied on the general heterogeneous local-to-nonlocal (LtN) coupling problems when there is large jump in physical (diffusivity) properties across the local-nonlocal interface Γ_i . Further details of the local and nonlocal problems will be described in Sections 2.1 and 2.2, respectively, and we leave the discussions of Robin transmission conditions on the coupling interface to a later Section 3.

2.1. Nonlocal Heat Problem

For the nonlocal subproblem we study compactly supported nonlocal integro-differential equations (IDEs) with radial kernels:

$$\begin{aligned}
\dot{u}_{nl,\delta}(\mathbf{x}, t) - \alpha_{nl} \mathcal{L}_\delta u_{nl,\delta}(\mathbf{x}, t) &= f_{nl}(\mathbf{x}, t), \quad \mathbf{x} \in \Omega_{nl} \\
u_{nl,\delta}(\mathbf{x}, t) &= u_{nl}^D(\mathbf{x}, t), \quad \mathbf{x} \in B\Omega_d \\
u_{nl,\delta}(\mathbf{x}, 0) &= u^{IC}(\mathbf{x}), \quad \mathbf{x} \in \Omega_{nl} \\
\text{where } \mathcal{L}_\delta u_{nl,\delta}(\mathbf{x}, t) &:= 2 \int_{B(\mathbf{x}, \delta)} J_\delta(|\mathbf{x} - \mathbf{y}|) (u_{nl,\delta}(\mathbf{y}, t) - u_{nl,\delta}(\mathbf{x}, t)) d\mathbf{y}.
\end{aligned} \tag{2.1}$$

Here $B(\mathbf{x}, \delta)$ is the ball centered at \mathbf{x} with radius δ , $u_{nl,\delta}(\mathbf{x}, t)$ is the nonlocal solution, $\dot{u}_{nl,\delta}$ is the first derivative in time of $u_{nl,\delta}$, α_{nl} denotes the diffusivity coefficient for Ω_{nl} , and $f_{nl}(\mathbf{x}, t)$, $u_{nl}^D(\mathbf{x}, t)$ are given data and nonlocal Dirichlet boundary condition, respectively. $u^{IC}(\mathbf{x})$ is the initial condition. The kernel function $J_\delta : \mathbb{R} \rightarrow \mathbb{R}$ is parameterized by a positive horizon parameter δ which measures the extent of nonlocal interaction. In this nonlocal setting every point in a domain interacts with a neighborhood Euclidean ball of surrounding points $B(\mathbf{x}, \delta)$. Therefore, the external boundary conditions are no longer prescribed on a sharp interface $\partial\Omega_{nl}$, but on a layer of thickness δ surrounding the domain that we refer to as $B\Omega_d$.

In this paper we further take a popular choice of J_δ as a rescaled kernel given by [52]

$$J_\delta(|\xi|) = \frac{1}{\delta^4} J\left(\frac{|\xi|}{\delta}\right), \tag{2.2}$$

where $J : [0, \infty) \rightarrow [0, \infty)$ is a nonnegative integrable function with $\int_{\mathbb{R}^2} J(|\mathbf{z}|) |\mathbf{z}|^2 d\mathbf{z} = 2$. Similar as in [49], we assume that $J(r)$ is nonincreasing in r , strictly positive in $r \in [0, 1]$ and vanishes when $r > 1$. It can be shown that at the limit of vanishing nonlocality, i.e. as $\delta \rightarrow 0$, the above nonlocal diffusion operator J_δ converges to the classical Laplacian Δ operator (see, e.g. [49, 56]):

$$\mathcal{L}_\delta v(\mathbf{x}) = \Delta v(\mathbf{x}) + \mathcal{O}(\delta^2) D^{(4)} v(\mathbf{x}), \tag{2.3}$$

where v is a sufficiently smooth function and $D^{(4)}$ is a combination of the fourth-order derivatives of v . Examples of properly scaled kernels in 2D include

$$J_\delta^1(r) = \begin{cases} \frac{4}{\pi\delta^4}, & \text{for } r \leq \delta; \\ 0, & \text{for } r > \delta; \end{cases} \quad \text{and} \quad J_\delta^2(r) = \begin{cases} \frac{3}{\pi\delta^3 r}, & \text{for } r \leq \delta; \\ 0, & \text{for } r > \delta. \end{cases}$$

To discretize the nonlocal subproblem spatially, we employ a meshfree quadrature rule based on the generalized moving least squares (GMLS) approximation framework [55]. In the following we consider the Dirichlet-type boundary conditions only, leaving the Robin-type boundary condition on Γ_i to Section 3. The nonlocal subdomain Ω_{nl} and

the nonlocal volumetric boundary $B\Omega_d$ are discretized by a collection of points $\chi_h = \{\mathbf{x}_i\}_{i=1,2,\dots,N_p} \subset \Omega_{nl} \cup B\Omega_d$, where the fill distance

$$h := \sup_{\mathbf{x}_i \in \chi_h} \min_{1 \leq j \leq N_p, j \neq i} |\mathbf{x}_i - \mathbf{x}_j| \quad (2.4)$$

is a length scale characterizing the resolution of the point cloud, and N_p denotes the total number of points. Similar as in [56], here we assume that the point set is quasi-uniform. For each point $\mathbf{x}_i \in \chi_h$, denoting the set of indices for points in $B(\mathbf{x}_i, \delta)$ as

$$I(\mathbf{x}_i) \equiv I(\mathbf{x}_i, \delta, \chi_h) := \{j \in \{1, \dots, N_p\} : |\mathbf{x}_i - \mathbf{x}_j| < \delta\}, \quad (2.5)$$

and $\#I(\mathbf{x}_i)$ as the number of indices in $I(\mathbf{x}_i)$, we then aim to reconstruct a degree m polynomial approximation $s_{u, \chi_h, i}(\mathbf{x}, t)$ for the nonlocal solution $u_{nl, \delta}(\mathbf{x}, t)$ in $B(\mathbf{x}_i, \delta)$. Specifically, define as a basis for the m -th order polynomial space $\pi_m(\mathbb{R}^2)$ the set $\{p_1(\mathbf{x}), p_2(\mathbf{x}), \dots, p_Q(\mathbf{x})\}$, $s_{u, \chi_h, i}$ is the solution to the optimization problem

$$s_{u, \chi_h, i}(\mathbf{x}, t) = \arg \min_{p \in \pi_m(\mathbb{R}^2)} \left\{ \sum_{j=1}^{N_p} [u_{nl, \delta}(\mathbf{x}_j, t) - p(\mathbf{x}_j)]^2 w(\mathbf{x}_i, \mathbf{x}_j) \right\}, \quad (2.6)$$

where $w(\mathbf{x}, \mathbf{y})$ is a translation-invariant positive weight function with compact support δ :

$$w(\mathbf{x}, \mathbf{y}) := \Phi_\delta(\mathbf{x} - \mathbf{y}) = \begin{cases} (1 - \frac{|\mathbf{x} - \mathbf{y}|}{\delta})^4, & \text{when } |\mathbf{x} - \mathbf{y}| \leq \delta, \\ 0 & \text{when } |\mathbf{x} - \mathbf{y}| > \delta. \end{cases}$$

Here we note that for a quasi-uniform pointset with sufficiently large ratio δ/h , the optimization problem possesses a unique solution [61]

$$s_{u, \chi_h, i}(\mathbf{x}, t) = \tilde{u}_\delta(t) DP(P^T DP)^{-1} R(\mathbf{x}), \quad (2.7)$$

where

$$\begin{aligned} \tilde{u}_\delta(t) &:= (u_{nl, \delta}(\mathbf{x}_j, t) : j \in I(\mathbf{x}_i))^T \in \mathbb{R}^{\#I(\mathbf{x}_i)}, & P &:= (p_k(\mathbf{x}_j))_{j \in I(\mathbf{x}_i), 1 \leq k \leq Q} \in \mathbb{R}^{\#I(\mathbf{x}_i) \times Q}, \\ D &:= \text{diag}(\Phi_\delta(\mathbf{x}_i - \mathbf{x}_j) : j \in I(\mathbf{x}_i)) \in \mathbb{R}^{\#I(\mathbf{x}_i) \times \#I(\mathbf{x}_i)}, & R(\mathbf{x}) &:= (p_1(\mathbf{x}), \dots, p_Q(\mathbf{x}))^T \in \mathbb{R}^Q. \end{aligned}$$

Note that when $u_{nl, \delta} \in \pi_m(\mathbb{R}^2)$, the above reconstruction is exact, i.e., $s_{u, \chi_h, i}(\mathbf{x}, t) = u_{nl, \delta}(\mathbf{x}, t)$. We then employ the reconstruction to evaluate the nonlocal model in (2.1) and obtained the semi-discretized formulation for $\tilde{u}_\delta(t)$:

$$\dot{u}_{nl, \delta}(\mathbf{x}_i, t) - 2\alpha_{nl} \tilde{u}_\delta(t) DP(P^T DP)^{-1} \int_{B(\mathbf{x}_i, \delta)} J_\delta(|\mathbf{y} - \mathbf{x}_i|) (R(\mathbf{y}) - R(\mathbf{x}_i)) d\mathbf{y} = f_{nl}(\mathbf{x}_i, t). \quad (2.8)$$

For further details on analysis and implementation of the meshfree quadrature rule we refer the interested readers to the previous work [55, 56], where we have employed this meshfree quadrature rule to develop asymptotically compatible spatial discretizations for static nonlocal diffusion model and peridynamics. To discretize (2.8) in time, in this paper

we employ the backward Euler scheme for simplicity and solve for $(U_\delta)_j^k \approx u_{nl,\delta}(\mathbf{x}_j, t^k)$ with:

$$\frac{1}{\Delta t}((U_\delta)_i^{k+1} - (U_\delta)_i^k) - 2\alpha_{nl}\tilde{u}_\delta^{k+1}DP(P^TDP)^{-1} \int_{B(\mathbf{x}_i,\delta)} J_\delta(|\mathbf{y} - \mathbf{x}_i|)(R(\mathbf{y}) - R(\mathbf{x}_i))d\mathbf{y} = f_{nl}(\mathbf{x}_i, t^{k+1}), \quad (2.9)$$

with Dirichlet boundary condition $(U_\delta)_j^k = u_{nl}^D(\mathbf{x}_j, t^k)$ for $\mathbf{x}_j \in B\Omega_d$. Here $\tilde{u}_\delta^k = ((U_\delta)_j^k : j \in I(\mathbf{x}_i))^T \in \mathbb{R}^{\#I(\mathbf{x}_i)}$. In the following we refer the nonlocal numerical solution with spatial discretization length scale h at the M -th time step as $u_{nl,\delta}^{M,h}$.

2.2. Local Heat Problem

For the local subproblem we consider the classical heat equation

$$\begin{aligned} \dot{u}_l(\mathbf{x}, t) - \alpha_l \Delta u_l(\mathbf{x}, t) &= f_l(\mathbf{x}, t), \quad \mathbf{x} \in \Omega_l \\ u_l(\mathbf{x}, t) &= u_l^D(\mathbf{x}, t), \quad \mathbf{x} \in \Gamma_d \\ u_l(\mathbf{x}, 0) &= u^{IC}(\mathbf{x}), \quad \mathbf{x} \in \Omega_l \end{aligned} \quad (2.10)$$

where $u_l(\mathbf{x}, t)$ is the local solution, \dot{u}_l is the first derivative of u_l in time, α_l is the diffusivity in the local region, u^{IC} is the initial condition, $f_l(\mathbf{x}, t)$ is the given data, and $u_l^D(\mathbf{x}, t)$ is the given Dirichlet boundary condition on the 1D external boundary Γ_d . Note that for coupling framework with overlapping regions such as [40], it usually requires $\alpha_l = \alpha_{nl}$ such that the nonlocal model will be equivalent with the local model as $\delta \rightarrow 0$. However, since in the current paper a nonoverlapping coupling framework is considered, it is possible that $\alpha_{nl} \neq \alpha_l$.

The local subproblem is solved with a finite element method code based on the FEniCS package [62, 63]. Spatially, with a test function v , when considering the Dirichlet boundary conditions only the local subproblem can be written into its weak form

$$\int_{\Omega_l} \dot{u}_l(\mathbf{x}, t)v(\mathbf{x})d\mathbf{x} + \alpha_l \int_{\Omega_l} \nabla u_l(\mathbf{x}, t) \cdot \nabla v(\mathbf{x})d\mathbf{x} = \int_{\Omega_l} f_l(\mathbf{x}, t)v(\mathbf{x})d\mathbf{x}, \quad \forall v \in \mathbf{W}_0, \quad (2.11)$$

where the solution $u_l(\mathbf{x}, t) \in \mathbf{W} = \{w(\mathbf{x}) \in H^1(\Omega_l) | w(\mathbf{x}) = u_l^D(\mathbf{x}, t) \text{ on } \Gamma_d\}$ and $\mathbf{W}_0 = \{w(\mathbf{x}) \in H^1(\Omega_l) | w(\mathbf{x}) = 0 \text{ on } \Gamma_d\}$. Ω_l is discretized with a regular quasi-uniform triangulation $\mathcal{T}_h(\Omega_l)$ of mesh size $h = \max_{T \in \mathcal{T}_h(\Omega_l)} h_T$, and the local solution u_l is approximated by continuous linear finite elements¹. With linear shape functions $\psi_p(\mathbf{x})$ for each element, the local solution $u_l(\mathbf{x}, t)$ and the test function $v_l(\mathbf{x})$ are expanded as

$$u_l(\mathbf{x}, t) = \sum_{p=1}^3 (U_l)_{ip}(t)\psi_p(\mathbf{x}), \quad v_l(\mathbf{x}) = \sum_{p=1}^3 (V_l)_{ip}\psi_p(\mathbf{x}),$$

¹Because the partitioned procedure is employed, the proposed framework can also be applied to the case when the two subdomain are discretized with different discretization length scales, i.e., $h_{nl} \neq h_l$. However, in this paper we demonstrate the method and results for $h_{nl} = h_l = h$ unless otherwise stated.

where $(U_l)_{ip}(t)$ and $(V_l)_{ip}$ are the expansion coefficients and ip is the global index of the coefficient. Substituting the above expansions into the weak formulation (2.11) and assembling globally, we obtain

$$M_l \dot{\mathbf{U}}_l(t) + B_l \mathbf{U}_l(t) = \mathbf{F}_l(t).$$

Here \mathbf{U}_l is the global vector of unknown expansion coefficients, \mathbf{F}_l is the global vector of the external loads, M_l is the mass matrix and B_l is the stiffness matrix. We then employ the backward Euler scheme for time integration and solve for $(\mathbf{U}_l)^{k+1}$:

$$\frac{M_l}{\Delta t}(\mathbf{U}_l^{k+1} - \mathbf{U}_l^k) + B_l \mathbf{U}_l^{k+1} = \mathbf{F}_l^{k+1}, \quad (2.12)$$

at the k -th time step. In the following we denote the local numerical solution with mesh size h at the M -th time step as $u_l^{M,h}$.

3. Boundary Conditions for Nonlocal Problems

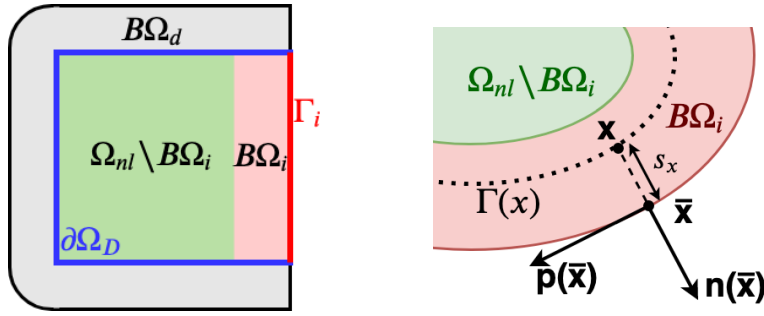


Figure 2: Notations for the Neumann and Robin-type boundary conditions in the nonlocal subdomain, where the nonlocal subdomain Ω_{nl} is represented by the green and red regions together. Nonlocal Dirichlet boundary condition is given on $B\Omega_d$, and nonlocal Robin transmission condition is applied on the red region $B\Omega_i$. On the corresponding local limit, Dirichlet boundary condition is given on $\partial\Omega_D$ and Robin transmission condition is applied on Γ_i . Right: Notations for the projection of point $\mathbf{x} \in B\Omega_i$, the corresponding unit tangential vector $\mathbf{p}(\bar{\mathbf{x}})$ and the unit normal vector $\mathbf{n}(\bar{\mathbf{x}})$.

In this section, we consider the nonlocal subproblem only, with problem setting as shown in Figure 2. Given that $\Omega_{nl} \in \mathbb{R}^2$ is a bounded, convex, connected and C^3 domain, β is the Robin coefficient, we seek a nonlocal analogue to the local Robin boundary condition $\beta u(\mathbf{x}) + \frac{\partial u}{\partial \mathbf{n}}(\mathbf{x}) = g(\mathbf{x})$, $\mathbf{x} \in \Gamma_i$ in the following corresponding classical problem

$$\begin{aligned} \dot{u}_0(\mathbf{x}, t) - \alpha_{nl} \Delta u_0(\mathbf{x}, t) &= f_{nl}(\mathbf{x}, t), \quad \mathbf{x} \in \Omega_{nl} \\ \beta u_0(\mathbf{x}, t) + \frac{\partial u_0}{\partial \mathbf{n}}(\mathbf{x}, t) &= g(\mathbf{x}, t), \quad \text{on } \Gamma_i \\ u_0(\mathbf{x}, t) &= u_{nl}^D(\mathbf{x}, t), \quad \mathbf{x} \in \partial\Omega_D \\ u_0(\mathbf{x}, 0) &= u^{IC}(\mathbf{x}), \quad \mathbf{x} \in \Omega_{nl}. \end{aligned} \quad (3.1)$$

Here we assume that the body load, boundary conditions and initial conditions satisfy proper consistency conditions. As shown in Figure 2, here $\mathbf{n}(\mathbf{x})$ is the unit exterior normal to Ω at \mathbf{x} , $\mathbf{p}(\mathbf{x})$ is the unit tangential vector with orientation clockwise to $\mathbf{n}(\mathbf{x})$, $\partial\Omega_D$ and Γ_i are both 1D curves with classical Dirichlet and Robin-type boundary conditions defined on them, respectively. Nonlocal Dirichlet-type constraint is applied on $B\Omega_d = \{\mathbf{x} \in \mathbb{R}^2 \setminus \Omega_{nl} : \text{dist}(\mathbf{x}, \partial\Omega_D) \leq \delta\}$. In the analysis of this section, we assume $u(\mathbf{x}) = 0$ on $B\Omega_d$ without loss of generality. Similarly, to apply the Robin-type constraint on Γ_i , we denote $B\Omega_i = \{\mathbf{x} \in \Omega_{nl} : \bar{\mathbf{x}} \in \Gamma_i, \text{dist}(\mathbf{x}, \Gamma_i) \leq \delta\}$. Here we assume sufficient regularity of the boundary (e.g., that it satisfies the hypotheses of the ϵ -neighborhood theorem from differential geometry) that we may take δ sufficiently small so that for any $\mathbf{x} \in \Omega$ within distance δ to Γ_i , there exists a unique orthogonal projection of \mathbf{x} onto Γ_i . We denote this projection as $\bar{\mathbf{x}}$. Therefore, one has $\bar{\mathbf{x}} - \mathbf{x} = s_{\bar{\mathbf{x}}} \mathbf{n}(\bar{\mathbf{x}})$ for $\mathbf{x} \in B\Omega_i$, where $0 \leq s_{\bar{\mathbf{x}}} \leq \delta$. We also assume that for $\mathbf{x} \in B\Omega_i$, we can find a contour $\Gamma(\mathbf{x})$ which is parallel to Γ_i (i.e., a level-set of a signed distance function), as shown in the right plot of Figure 2. In the following contents, we denote \mathbf{x}_l as the point with distance l to \mathbf{x} along $\Gamma(\mathbf{x})$ following the $\mathbf{p}(\bar{\mathbf{x}})$ direction, and \mathbf{x}_{-l} as the point with distance l to \mathbf{x} in the opposite direction. Moreover, we employ the following notations for the directional components of the Hessian matrix of a scalar function v :

$$[v(\mathbf{x})]_{pp} := \mathbf{p}^T(\bar{\mathbf{x}})[\nabla \circ \nabla v(\mathbf{x})]\mathbf{p}(\bar{\mathbf{x}}), \quad [v(\mathbf{x})]_{nn} := \mathbf{n}^T(\bar{\mathbf{x}})[\nabla \circ \nabla v(\mathbf{x})]\mathbf{n}(\bar{\mathbf{x}}), \quad [v(\mathbf{x})]_{pn} := \mathbf{p}^T(\bar{\mathbf{x}})[\nabla \circ \nabla v(\mathbf{x})]\mathbf{n}(\bar{\mathbf{x}}),$$

and the higher order derivative components are similarly defined.

With the above notations and assumptions, in this section we first introduce a nonlocal Neumann boundary condition in Section 3.1, then estimate the order of convergence rate to the corresponding local limit. With the Neumann-type boundary condition, we then propose a new generalization of classical Robin condition for nonlocal problems in Section 3.2. To verify the asymptotic convergence of the proposed boundary treatment, we discretize the proposed Robin-type constraint problem with the meshfree quadrature rule [55, 56] in Section 3.3, then use numerical examples to demonstrate the convergence of the discrete model to the analytical local limit as the discretization length scale h , time step size Δt and the nonlocal interaction length scale δ all vanish simultaneously.

3.1. A Nonlocal Neumann-Type Boundary Condition

When $\beta = 0$, in (3.1) the Neumann boundary condition is imposed on Γ_i . Inspired by [49, 53, 56], we propose the nonlocal Neumann-type boundary condition by firstly considering the following modification for $\mathbf{x} \in B\Omega_i$:

$$\begin{aligned} \dot{u}_{nl,\delta}(\mathbf{x}, t) - 2\alpha_{nl} \int_{\Omega_{nl}} J_\delta(|\mathbf{x} - \mathbf{y}|)(u_{nl,\delta}(\mathbf{y}, t) - u_{nl,\delta}(\mathbf{x}, t))d\mathbf{y} - \alpha_{nl} \int_{\mathbb{R}^2 \setminus \Omega_{nl}} J_\delta(|\mathbf{x} - \mathbf{y}|)(\mathbf{y} - \mathbf{x}) \cdot \mathbf{n}(\bar{\mathbf{x}})(g(\mathbf{x}, t) + g(\mathbf{y}, t))d\mathbf{y} \\ - \alpha_{nl} \int_{\mathbb{R}^2 \setminus \Omega_{nl}} J_\delta(|\mathbf{x} - \mathbf{y}|)|(\mathbf{y} - \mathbf{x}) \cdot \mathbf{p}(\bar{\mathbf{x}})|^2 d\mathbf{y}[u_{nl,\delta}(\mathbf{x}, t)]_{pp} = f_{nl}(\mathbf{x}, t). \end{aligned} \quad (3.2)$$

The last two terms on the left hand side of the above formulation provide an approximation to

$$-2\alpha_{nl} \int_{\mathbb{R}^2 \setminus \Omega_{nl}} J_\delta(|\mathbf{x} - \mathbf{y}|)(u_{nl,\delta}(\mathbf{y}, t) - u_{nl,\delta}(\mathbf{x}, t))d\mathbf{y},$$

which account for the contributions from material points outside the nonlocal domain [53, 64]. To apply the Robin transmission condition $g(\mathbf{x}, t)$ which is defined only on the sharp interface Γ_i , the $g(\mathbf{x}, t)$ and $g(\mathbf{y}, t)$ terms in (3.2) will be approximated with the following (local) extensions

$$\begin{aligned} g(\mathbf{x}, t) &\approx g(\bar{\mathbf{x}}, t) + \frac{1}{\alpha_{nl}}(\mathbf{x} - \bar{\mathbf{x}}) \cdot \mathbf{n}(\bar{\mathbf{x}})(\dot{u}_{nl,\delta}(\mathbf{x}, t) - f_{nl}(\mathbf{x}, t)) - (\mathbf{x} - \bar{\mathbf{x}}) \cdot \mathbf{n}(\bar{\mathbf{x}})[u_{nl,\delta}(\mathbf{x}, t)]_{pp}, \\ g(\mathbf{y}, t) &\approx g(\bar{\mathbf{x}}, t) + \frac{1}{\alpha_{nl}}(\mathbf{y} - \bar{\mathbf{x}}) \cdot \mathbf{n}(\bar{\mathbf{x}})(\dot{u}_{nl,\delta}(\mathbf{x}, t) - f_{nl}(\mathbf{x}, t)) - (\mathbf{y} - \bar{\mathbf{x}}) \cdot \mathbf{n}(\bar{\mathbf{x}})[u_{nl,\delta}(\mathbf{x}, t)]_{pp}. \end{aligned}$$

Furthermore, we replace $[u_{nl,\delta}(\mathbf{x}, t)]_{pp}$ with its approximation $2 \int_{-\delta}^{\delta} H_{\delta}(|l|)(u_{nl,\delta}(\mathbf{x}_l, t) - u_{nl,\delta}(\mathbf{x}, t))d\mathbf{x}_l - \kappa(\bar{\mathbf{x}})g(\bar{\mathbf{x}}, t)$. Here $d\mathbf{x}_l$ is the line integral along the contour $\Gamma(\mathbf{x})$, $\kappa(\bar{\mathbf{x}})$ is the curvature of $\partial\Omega_{nl}$ at $\bar{\mathbf{x}}$, and $H_{\delta}(|r|) = \frac{1}{\delta^3}H\left(\frac{|r|}{\delta}\right)$ is the kernel for 1D nonlocal diffusion model such that $H : [0, \infty) \rightarrow [0, \infty)$ is a nonnegative and continuous function with $\int_{\mathbb{R}} H(|z|)|z|^2 dz = 1$. $H(r)$ is nonincreasing in r , strictly positive in $[0, 1]$ and vanishes for $|z| > 1$. Moreover, we add a further requirement on H that $\int_{\mathbb{R}} H(z)dz := C_H < \infty$. Substituting the above two approximations into (3.2), we obtain the following model

$$\begin{aligned} &Q_{\delta}(\mathbf{x})\dot{u}_{nl,\delta}(\mathbf{x}, t) - 2\alpha_{nl} \int_{\Omega_{nl}} J_{\delta}(|\mathbf{x} - \mathbf{y}|)(u_{nl,\delta}(\mathbf{y}, t) - u_{nl,\delta}(\mathbf{x}, t))d\mathbf{y} - 2\alpha_{nl}M_{\delta}(\mathbf{x}) \int_{-\delta}^{\delta} H_{\delta}(|l|)(u_{nl,\delta}(\mathbf{x}_l, t) - u_{nl,\delta}(\mathbf{x}, t))d\mathbf{x}_l \\ &= Q_{\delta}(\mathbf{x})f_{nl}(\mathbf{x}, t) + \alpha_{nl}V_{\delta}(\mathbf{x})g(\bar{\mathbf{x}}, t) \end{aligned}$$

where

$$Q_{\delta}(\mathbf{x}) := 1 - \int_{\mathbb{R}^2 \setminus \Omega_{nl}} J_{\delta}(|\mathbf{x} - \mathbf{y}|) \left[|(\mathbf{y} - \bar{\mathbf{x}}) \cdot \mathbf{n}(\bar{\mathbf{x}})|^2 - |(\mathbf{x} - \bar{\mathbf{x}}) \cdot \mathbf{n}(\bar{\mathbf{x}})|^2 \right] d\mathbf{y}, \quad (3.3)$$

$$V_{\delta}(\mathbf{x}) := 2 \int_{\mathbb{R}^2 \setminus \Omega_{nl}} J_{\delta}(|\mathbf{x} - \mathbf{y}|)(\mathbf{y} - \mathbf{x}) \cdot \mathbf{n}(\bar{\mathbf{x}})d\mathbf{y} - M_{\delta}(\mathbf{x})\kappa(\bar{\mathbf{x}}), \quad (3.4)$$

$$M_{\delta}(\mathbf{x}) := \int_{\mathbb{R}^2 \setminus \Omega_{nl}} J_{\delta}(|\mathbf{x} - \mathbf{y}|) \left[|(\mathbf{y} - \mathbf{x}) \cdot \mathbf{p}(\bar{\mathbf{x}})|^2 - |(\mathbf{y} - \bar{\mathbf{x}}) \cdot \mathbf{n}(\bar{\mathbf{x}})|^2 + |(\mathbf{x} - \bar{\mathbf{x}}) \cdot \mathbf{n}(\bar{\mathbf{x}})|^2 \right] d\mathbf{y}. \quad (3.5)$$

Thus, by defining the nonlocal operator:

$$L_{N\delta}u := 2 \int_{\Omega_{nl}} J_{\delta}(|\mathbf{x} - \mathbf{y}|)(u(\mathbf{y}, t) + u(\mathbf{x}, t))d\mathbf{y} + 2M_{\delta}(\mathbf{x}) \int_{-\delta}^{\delta} H_{\delta}(|l|)(u(\mathbf{x}_l, t) - u(\mathbf{x}, t))d\mathbf{x}_l \quad (3.6)$$

in problems with Neumann-type boundary conditions we obtain the following proposed nonlocal formulation

$$\begin{aligned} &\dot{u}_{nl,\delta}(\mathbf{x}, t) - \alpha_{nl}\mathcal{L}_{\delta}u_{nl,\delta}(\mathbf{x}, t) = f_{nl}(\mathbf{x}, t), \quad \mathbf{x} \in \Omega_{nl} \setminus B\Omega_i \\ &Q_{\delta}(\mathbf{x})\dot{u}_{nl,\delta}(\mathbf{x}, t) - \alpha_{nl}\mathcal{L}_{N\delta}u_{nl,\delta}(\mathbf{x}, t) = Q_{\delta}(\mathbf{x})f_{nl}(\mathbf{x}, t) + \alpha_{nl}V_{\delta}(\mathbf{x})g(\bar{\mathbf{x}}, t), \quad \mathbf{x} \in B\Omega_i \\ &u_{nl,\delta}(\mathbf{x}, t) = u_{nl}^D(\mathbf{x}, t), \quad \mathbf{x} \in B\Omega_d \\ &u_{nl,\delta}(\mathbf{x}, 0) = u^{IC}(\mathbf{x}). \quad \mathbf{x} \in \Omega_{nl} \end{aligned} \quad (3.7)$$

The corresponding nonlocal energy seminorm $\|\cdot\|_{S_\delta}$ is given by

$$\|v\|_{S_\delta(\Omega_{nl})}^2 = \int_{\Omega_{nl}} \int_{\Omega_{nl}} J_\delta(|\mathbf{x} - \mathbf{y}|) [v(\mathbf{y}) - v(\mathbf{x})]^2 d\mathbf{y} d\mathbf{x} + \int_{B\Omega_i} M_\delta(\mathbf{x}) \int_{-\delta}^\delta H_\delta(|l|) [v(\mathbf{x}_l) - v(\mathbf{x})]^2 d\mathbf{x}_l d\mathbf{x}$$

which defines the energy space²

$$S_\delta(\Omega_{nl}) = \left\{ v \in L^2(\Omega_{nl}) : \|v\|_{S_\delta(\Omega_{nl})} < \infty \right\}.$$

We now develop the analysis for homogeneous Neumann-type constraints, i.e., $g(\mathbf{x}, t) = 0$. Throughout this section, we consider the symbol “ C ” to indicate a generic constant that is independent of δ , but may have different numerical values in different situations. Moreover, we make a critical geometric assumption for the simplicity of analysis (as illustrated by the left plot of Figure 3): let $\{\mathbf{z}_1, \mathbf{z}_2\} := \partial\Omega_D \cap \Gamma_i$, $\pi_{\partial\Omega_{nl}}$ be the projection operator onto $\partial\Omega_{nl} = \partial\Omega_D \cup \Gamma_i$, and $\tau(\mathbf{z}_1)$ (resp. $\tau(\mathbf{z}_2)$) be the tangent line to $\partial\Omega_{nl}$ at \mathbf{z}_1 (resp. \mathbf{z}_2), then we assume that the intersecting point $\tilde{\mathbf{z}} := \tau(\mathbf{z}_1) \cap \tau(\mathbf{z}_2)$ satisfies $\pi_{\partial\Omega_{nl}}(\tilde{\mathbf{z}}) \in \Gamma_i$. Here we note that due to the convexity of Ω_{nl} , the map $\pi_{\partial\Omega_{nl}}(\mathbf{x})$ is always well defined and single-valued for any point $\mathbf{x} \notin \Omega_{nl}$.

Remark 1. When Γ_i is flat, $\tau(\mathbf{z}_1)$ and $\tau(\mathbf{z}_2)$ coincide. One can take the intersection point $\tilde{\mathbf{z}}$ as any point on Γ_i , and the analysis below still holds true.

With the analysis in [56, Lemma 3.1], we note that there exists a $\bar{\delta} > 0$ such that for $\delta \leq \bar{\delta}$, $\mathbf{x} \in B\Omega_i$ we have $0 \leq M_\delta(\mathbf{x}) \leq C$. Moreover, with the geometric assumptions on Ω_{nl} we have bounds for $Q_\delta(\mathbf{x})$:

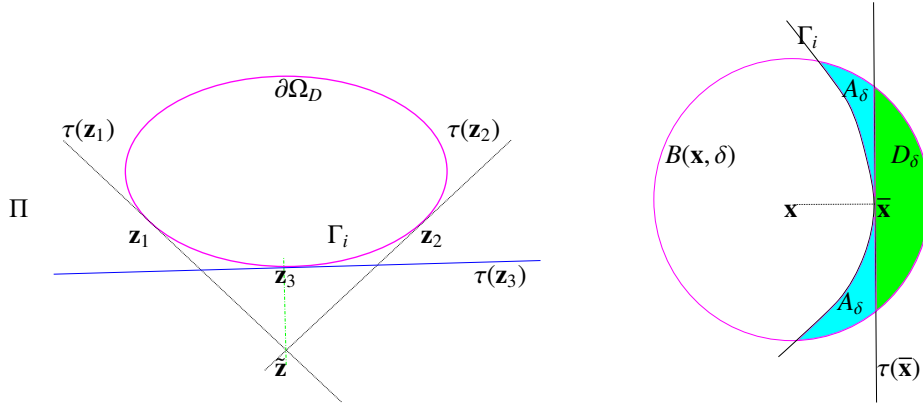


Figure 3: Notation for the geometric estimates in Section 3.2. Left: illustration of the geometric assumption and notation for the barrier function $\phi(\mathbf{x})$ definition in Theorem 1. Right: regions in Lemma 3.1. Green represents D_δ , the region in $B(\mathbf{x}, \delta)$ which lies on the other side of the tangential line at $\bar{\mathbf{x}}$ with respect to Ω_{nl} . Cyan represents A_δ , the region in $B_\delta(\mathbf{x})$ which lies between $\mathbb{R}^2 \setminus \Omega_{nl}$ and the tangential line.

²We note that for a fixed δ and integrable kernels J, H , based on the results in [56, 65–67] we have

$$\|u\|_{L^2(\Omega_{nl})} \leq C_1 \|u\|_{S_\delta(\Omega_{nl})} \leq C_2(\delta) \|u\|_{L^2(\Omega_{nl})},$$

where $C_1, C_2(\delta)$ are constants independent of u but $C_2(\delta)$ depends on δ . Therefore, $S_\delta(\Omega)$ is equivalent to the space of $L^2(\Omega)$ functions.

Lemma 3.1. *Let $\Omega_{nl} \in \mathbb{R}^2$ be a convex and C^3 domain, then there exists $\bar{\delta} > 0$ such that for $0 < \delta \leq \bar{\delta}$, $Q_\delta(\mathbf{x})$ is bounded from above and below independent of δ . Specifically, $0 < \frac{1}{2} - C_q\delta \leq Q_\delta(\mathbf{x}) \leq \frac{3}{2} + C_q\delta$ where $C_q > 0$ is a constant independent of δ .*

Proof. As shown in the right plot of Figure 3, we note that

$$Q_\delta(\mathbf{x}) = 1 - \int_{D_\delta} J_\delta(|\mathbf{x} - \mathbf{y}|) \left[|(\mathbf{y} - \bar{\mathbf{x}}) \cdot \mathbf{n}(\bar{\mathbf{x}})|^2 - |(\mathbf{x} - \bar{\mathbf{x}}) \cdot \mathbf{n}(\bar{\mathbf{x}})|^2 \right] d\mathbf{y} - \int_{A_\delta} J_\delta(|\mathbf{x} - \mathbf{y}|) \left[|(\mathbf{y} - \bar{\mathbf{x}}) \cdot \mathbf{n}(\bar{\mathbf{x}})|^2 - |(\mathbf{x} - \bar{\mathbf{x}}) \cdot \mathbf{n}(\bar{\mathbf{x}})|^2 \right] d\mathbf{y}.$$

With $\tau(\bar{\mathbf{x}})$ representing the tangent line to Γ_i at $\bar{\mathbf{x}}$, here D_δ is the region of $B(\mathbf{x}, \delta)$ on the side of $\tau(\bar{\mathbf{x}})$ not containing Ω_{nl} (as shown in the green region of Figure 3), and $A_\delta := B(\mathbf{x}, \delta) \setminus (D_\delta \cup \Omega_{nl})$ (as shown in the cyan region of Figure 3). We consider first the D_δ part. When $\mathbf{y} \in D_\delta$, we note that $|(\mathbf{y} - \mathbf{x}) \cdot \mathbf{n}(\bar{\mathbf{x}})|^2 \geq |(\mathbf{x} - \bar{\mathbf{x}}) \cdot \mathbf{n}(\bar{\mathbf{x}})|^2$ and $|(\mathbf{y} - \mathbf{x}) \cdot \mathbf{n}(\bar{\mathbf{x}})|^2 \geq |(\mathbf{y} - \bar{\mathbf{x}}) \cdot \mathbf{n}(\bar{\mathbf{x}})|^2$, therefore

$$\begin{aligned} \int_{D_\delta} J_\delta(|\mathbf{x} - \mathbf{y}|) \left[|(\mathbf{y} - \bar{\mathbf{x}}) \cdot \mathbf{n}(\bar{\mathbf{x}})|^2 - |(\mathbf{x} - \bar{\mathbf{x}}) \cdot \mathbf{n}(\bar{\mathbf{x}})|^2 \right] d\mathbf{y} &\geq - \int_{D_\delta} J_\delta(|\mathbf{x} - \mathbf{y}|) |(\mathbf{y} - \mathbf{x}) \cdot \mathbf{n}(\bar{\mathbf{x}})|^2 d\mathbf{y} \geq -\frac{1}{2}. \\ \int_{D_\delta} J_\delta(|\mathbf{x} - \mathbf{y}|) \left[|(\mathbf{y} - \bar{\mathbf{x}}) \cdot \mathbf{n}(\bar{\mathbf{x}})|^2 - |(\mathbf{x} - \bar{\mathbf{x}}) \cdot \mathbf{n}(\bar{\mathbf{x}})|^2 \right] d\mathbf{y} &\leq \int_{D_\delta} J_\delta(|\mathbf{x} - \mathbf{y}|) |(\mathbf{y} - \bar{\mathbf{x}}) \cdot \mathbf{n}(\bar{\mathbf{x}})|^2 d\mathbf{y} \leq \frac{1}{2}. \end{aligned}$$

For the A_δ region, similar as in [56, Lemma 3.1], it can be shown that the area of A_δ satisfies $|A_\delta| \leq C\delta^3$ since Ω_{nl} is a C^3 domain. Hence there exists a $\bar{\delta}$ such that for $\delta < \bar{\delta}$,

$$\left| \int_{A_\delta} J_\delta(|\mathbf{x} - \mathbf{y}|) \left[|(\mathbf{y} - \bar{\mathbf{x}}) \cdot \mathbf{n}(\bar{\mathbf{x}})|^2 - |(\mathbf{x} - \bar{\mathbf{x}}) \cdot \mathbf{n}(\bar{\mathbf{x}})|^2 \right] d\mathbf{y} \right| \leq C_q\delta,$$

$$\text{and } \frac{1}{2} - C_q\delta \leq Q_\delta(\mathbf{x}) \leq \frac{3}{2} + C_q\delta. \quad \square$$

For problem (3.7) we have the nonlocal maximum principle stated below

Lemma 3.2. *For $u \in C^1(0, T; C(\overline{\Omega_{nl}}) \cap C(B\Omega_d)) \cup C([0, T] \times \overline{\Omega_{nl}})$, $u(\mathbf{x}, t)$ bounded on $(\mathbf{x}, t) \in B\Omega_d \times [0, T]$, assuming that u satisfies $\dot{u} - \alpha_{nl}L_\delta u \leq 0$ for all $x \in \Omega_{nl} \setminus B\Omega_i$ and $Q_\delta \dot{u} - \alpha_{nl}L_{N\delta} u \leq 0$ for all $x \in B\Omega_i$, we have*

$$\sup_{(\mathbf{x}, t) \in (\overline{\Omega_{nl}} \cup B\Omega_d) \times [0, T]} u(\mathbf{x}, t) \leq \max \left\{ \sup_{\mathbf{x} \in \overline{\Omega_{nl}} \cup B\Omega_d} u(\mathbf{x}, 0), \sup_{(\mathbf{x}, t) \in B\Omega_d \times [0, T]} u(\mathbf{x}, t) \right\}. \quad (3.8)$$

Proof. Assuming that (3.8) doesn't hold true, then there exists $(\mathbf{x}^*, t^*) \in (\Omega_{nl} \cup \Gamma_i) \times (0, T]$ such that $u(\mathbf{x}^*, t^*)$ achieves the maximum. One can then obtain a contradiction following a similar argument as [56]:

Case 1: if $\mathbf{x}^* \in \Omega_{nl} \setminus B\Omega_i$, then $\dot{u}(\mathbf{x}^*, t^*) \geq 0$, $-\alpha_{nl}\mathcal{L}_\delta u(\mathbf{x}^*, t^*) \geq 0$. Therefore, $\dot{u}(\mathbf{x}^*, t^*) = 0$ and $\mathcal{L}_\delta u(\mathbf{x}^*, t^*) = 0$. For all $\mathbf{y} \in (\overline{\Omega_{nl}} \cup B\Omega_d) \cap B(\mathbf{x}^*, \delta)$, $u(\mathbf{y}, t^*) = u(\mathbf{x}^*, t^*)$ achieves the maximum.

Case 2: if $\mathbf{x}^* \in B\Omega_i$, then $Q_\delta(\mathbf{x})\dot{u}(\mathbf{x}, t) \geq 0$, $-\alpha_{nl}\mathcal{L}_{N\delta} u(\mathbf{x}, t) \geq 0$. Therefore, $Q_\delta(\mathbf{x})\dot{u}(\mathbf{x}, t) = -\alpha_{nl}\mathcal{L}_{N\delta} u(\mathbf{x}, t) = 0$, and $u(\mathbf{y}, t^*) = u(\mathbf{x}^*, t^*)$ achieves the maximum for all $\mathbf{y} \in \overline{\Omega_{nl}} \cap B(\mathbf{x}^*, \delta)$.

We then apply the same arguments with \mathbf{y} in place of \mathbf{x}^* . This process can be repeated until the region where $u(\mathbf{z}, t^*) = \sup_{\overline{\Omega_{nl} \cup B\Omega_d}} u$ expands to the entire domain of $\overline{\Omega_{nl} \cup B\Omega_d}$. In other words, to have a global maximum inside Ω_{nl} , the only possibility is for $u(\cdot, t^*)$ to be constant on $\overline{\Omega_{nl} \cup B\Omega_d}$, which contradicts with the assumption. \square

Moreover, when considering a semi-discretized problem with backward Euler method:

$$\begin{aligned} \frac{1}{\Delta t}(u_{nl,\delta}^{k+1}(\mathbf{x}) - u_{nl,\delta}^k(\mathbf{x})) - \alpha_{nl}\mathcal{L}_\delta u_{nl,\delta}^{k+1}(\mathbf{x}) &= f_{nl}(\mathbf{x}, t^{k+1}), \quad \mathbf{x} \in \Omega_{nl} \setminus B\Omega_i \\ \frac{1}{\Delta t}Q_\delta(\mathbf{x})(u_{nl,\delta}^{k+1}(\mathbf{x}) - u_{nl,\delta}^k(\mathbf{x})) - \alpha_{nl}\mathcal{L}_{N\delta} u_{nl,\delta}^{k+1}(\mathbf{x}) &= Q_\delta(\mathbf{x})f_{nl}(\mathbf{x}, t^{k+1}) + \alpha_{nl}V_\delta(\mathbf{x})g(\bar{\mathbf{x}}, t^{k+1}), \quad \mathbf{x} \in B\Omega_i \\ u_{nl,\delta}^{k+1}(\mathbf{x}) &= u_{nl}^D(\mathbf{x}, t^{k+1}), \quad \mathbf{x} \in B\Omega_d \\ u_{nl,\delta}^0(\mathbf{x}) &= u^{IC}(\mathbf{x}). \quad \mathbf{x} \in \Omega_{nl} \end{aligned} \quad (3.9)$$

the nonlocal maximum principle also holds true:

Lemma 3.3. *For a sequence of semi-discretized solutions $\{u^k(\mathbf{x})\}$, $k = 0, 1, \dots, M$ where $M = \frac{T}{\Delta t}$, $u^k \in C(\overline{\Omega_{nl}}) \cap C(B\Omega_d)$, $u(\mathbf{x}, 0)$ is bounded on $\mathbf{x} \in \Omega_{nl}$ and $u^k(\mathbf{x})$ is bounded on $\mathbf{x} \in B\Omega_d$, assuming that u^k satisfies $\frac{1}{\Delta t}(u^{k+1} - u^k) - \alpha_{nl}L_\delta u^{k+1} \leq 0$ for all $\mathbf{x} \in \Omega_{nl} \setminus B\Omega_i$ and $\frac{1}{\Delta t}Q_\delta(u^{k+1} - u^k) - \alpha_{nl}L_{N\delta} u^{k+1} \leq 0$ for all $\mathbf{x} \in B\Omega_i$, we have*

$$\max_{k=0}^M \sup_{\mathbf{x} \in \overline{\Omega_{nl} \cup B\Omega_d}} u^k(\mathbf{x}) \leq \max \left\{ \sup_{\mathbf{x} \in \overline{\Omega_{nl} \cup B\Omega_d}} u(\mathbf{x}, 0), \max_{k=0}^M \sup_{\mathbf{x} \in B\Omega_d} u^k(\mathbf{x}) \right\}. \quad (3.10)$$

Proof. The argument is similarly obtained as in the proof of Lemma 3.2. \square

We now assume that $u_{nl,\delta}^k$ is the solution of (3.9) and u_0^k is the solution of semi-discretized local problem (3.1) with the backward Euler method. Denote $e_\delta^k(\mathbf{x}) := u_{nl,\delta}^k(\mathbf{x}) - u_0^k(\mathbf{x})$ and

$$\begin{aligned} T_\delta^k(\mathbf{x}) &:= \alpha_{nl}(-\Delta u_0^k(\mathbf{x}) + L_\delta u_0^k(\mathbf{x})), & \text{for } \mathbf{x} \in \Omega_{nl} \setminus B\Omega_i, \\ T_\delta^k(\mathbf{x}) &:= \alpha_{nl}(-\Delta u_0^k(\mathbf{x}, t) + L_{N\delta} u_0^k(\mathbf{x})) + (Q_\delta(\mathbf{x}) - 1) \left(f_{nl}(\mathbf{x}, t^k) - \frac{1}{\Delta t}[u_0^k(\mathbf{x}) - u_0^{k-1}(\mathbf{x})] \right), & \text{for } \mathbf{x} \in B\Omega_i. \end{aligned}$$

Then for $\mathbf{x} \in \Omega_{nl} \setminus B\Omega_i$,

$$\frac{1}{\Delta t}(e_\delta^k(\mathbf{x}) - e_\delta^{k-1}(\mathbf{x})) - \alpha_{nl}L_\delta e_\delta^k(\mathbf{x}) = \alpha_{nl}(-\Delta u_0^k(\mathbf{x}) + L_\delta u_0^k(\mathbf{x})) = T_\delta^k(\mathbf{x}),$$

and for $\mathbf{x} \in B\Omega_i$,

$$\frac{1}{\Delta t}Q_\delta(\mathbf{x})(e_\delta^k(\mathbf{x}) - e_\delta^{k-1}(\mathbf{x})) - \alpha_{nl}L_{N\delta} e_\delta^k(\mathbf{x}) = Q_\delta(\mathbf{x})f_{nl}(\mathbf{x}, t^k) - \frac{1}{\Delta t}Q_\delta(\mathbf{x})(u_0^k(\mathbf{x}) - u_0^{k-1}(\mathbf{x})) + \alpha_{nl}L_{N\delta} u_0^k(\mathbf{x}) = T_\delta^k(\mathbf{x}).$$

In the following we take a specific kernel $J_\delta(s) = J_\delta^1(s) = \frac{4}{\pi\delta^4}$ for $s \leq \delta$ for simplicity. With Taylor expansion we can obtain the following truncation estimate for T_δ :

Lemma 3.4. *Suppose u_0^k is the solution to semi-discretized local problem (3.1), then*

$$\begin{aligned} |T_\delta^k(\mathbf{x})| &\leq C(T)(\delta^2), \quad \text{for } \mathbf{x} \in \Omega_{nl} \setminus B\Omega_i, \\ |T_\delta^k(\mathbf{x})| &\leq C(T)[\delta - s_{\mathbf{x}}]^{3/2}\delta^{-1/2} + O(\delta^2), \quad \text{for } \mathbf{x} \in B\Omega_i, \end{aligned}$$

where $C(T)$ is independent of δ but might depend on T .

Proof. The proof is based on the Taylor expansion of u_0 and an estimate for the asymmetric part in A_δ , similar as in [56, Lemma 4.2]. \square

Furthermore, with the maximum principle in Lemma 3.3, when f_{nl} and u_{nl}^D are both continuous we have the following lemma.

Lemma 3.5. *Suppose that a nonnegative continuous function $\phi(\mathbf{x})$ is defined on $\overline{\Omega_{nl}}$, and $L_\delta\phi \geq G(\mathbf{x}) > 0$ for $\mathbf{x} \in \Omega_{nl} \setminus B\Omega_i$, $L_{N\delta}\phi \geq G(\mathbf{x}) > 0$ for $\mathbf{x} \in B\Omega_i$. Then*

$$\max_{k=0}^M \sup_{\mathbf{x} \in \overline{\Omega_{nl}}} |e_\delta^k(\mathbf{x})| \leq \sup_{\mathbf{x} \in \overline{\Omega_{nl}} \cup B\Omega_d} \phi(\mathbf{x}) \max_{k=0}^M \sup_{\mathbf{x} \in \overline{\Omega_{nl}}} \frac{|T_\delta^k(\mathbf{x})|}{G(\mathbf{x})}. \quad (3.11)$$

Proof. The proof is obtained with the maximum principle: Let $K = \max_{k=0}^M \sup_{\mathbf{x} \in \overline{\Omega_{nl}}} \frac{|T_\delta^k(\mathbf{x})|}{G(\mathbf{x})}$, then for $K\phi(\mathbf{x}) + e_\delta^k(\mathbf{x})$ we have:

$$\frac{1}{\Delta t}(e_\delta^k(\mathbf{x}) - e_\delta^{k-1}(\mathbf{x})) - \alpha_{nl}L_\delta(K\phi(\mathbf{x}) + e_\delta^k(\mathbf{x})) = \alpha_{nl} \left[-\max_{k=0}^M \sup_{\mathbf{x} \in \overline{\Omega_{nl}}} \frac{|T_\delta^k(\mathbf{x})|}{G(\mathbf{x})} L_\delta\phi(\mathbf{x}) + T_\delta^k(\mathbf{x}) \right] \leq 0$$

for $\mathbf{x} \in \Omega_{nl} \setminus B\Omega_i$. A similar argument holds for $\mathbf{x} \in B\Omega_i$. With the maximum principle in Lemma 3.3 we have

$$\max_{k=0}^M \sup_{\mathbf{x} \in \overline{\Omega_{nl}}} e_\delta^k(\mathbf{x}) \leq \max_{k=0}^M \sup_{\mathbf{x} \in \overline{\Omega_{nl}}} (K\phi(\mathbf{x}) + e_\delta^k(\mathbf{x})) \leq K \max_{k=0}^M \sup_{\mathbf{x} \in \overline{\Omega_{nl}} \cup B\Omega_d} \phi(\mathbf{x}).$$

Similarly, we have $-\frac{1}{\Delta t}(e_\delta^k(\mathbf{x}) - e_\delta^{k-1}(\mathbf{x})) - \alpha_{nl}L_\delta(K\phi(\mathbf{x}) - e_\delta^k(\mathbf{x})) \leq 0$ for $\mathbf{x} \in \Omega_{nl} \setminus B\Omega_i$ and $-\frac{1}{\Delta t}(e_\delta^k(\mathbf{x}) - e_\delta^{k-1}(\mathbf{x})) - \alpha_{nl}L_{N\delta}(K\phi(\mathbf{x}) - e_\delta^k(\mathbf{x})) \leq 0$ for $\mathbf{x} \in B\Omega_i$, hence

$$\max_{k=0}^M \sup_{\mathbf{x} \in \overline{\Omega_{nl}}} (-e_\delta^k(\mathbf{x})) \leq \max_{k=0}^M \sup_{\mathbf{x} \in \overline{\Omega_{nl}}} (K\phi(\mathbf{x}) - e_\delta^k(\mathbf{x})) \leq K \max_{k=0}^M \sup_{\mathbf{x} \in \overline{\Omega_{nl}} \cup B\Omega_d} \phi(\mathbf{x}).$$

\square

With the above lemma and assuming that the datum has sufficient Hölder continuity, we obtain the following main theorem:

Theorem 1. Suppose $f_{nl} \in C^{1+\epsilon/2, \epsilon}((0, \infty) \times \mathbb{R}^2)$, $u_{nl}^D \in C^{2+\epsilon/2, 2+\epsilon}((0, \infty) \times (\overline{\Omega_{nl}} \cup B\Omega_d))$, $\frac{\partial u_{nl}^D}{\partial \mathbf{n}} = 0$ on Γ_i , $u^{IC} \in C^{2+\epsilon}(\mathbb{R}^2)$, and $\epsilon \in (0, 1)$, $\{u_{nl, \delta}^k(\mathbf{x})\}$ are the semi-discretized results from the backward Euler method to the nonlocal problem. Then for sufficiently small δ , there exists a constant C independent of δ such that

$$\sup_{\mathbf{x} \in \Omega_{nl}} |u_{nl, \delta}^M(\mathbf{x}) - u_0(\mathbf{x}, T)| \leq C(T)(\Delta t + \delta^2), \quad (3.12)$$

where $M = \frac{T}{\Delta t}$.

Proof. With the regularity of the given datum and the domain, we have $u_0(\mathbf{x}, t) \in C^{2+\epsilon/2, 2+\epsilon}((0, \infty) \times \Omega_{nl})$ (see, e.g., [68, Theorem 10.4.1]) and therefore $\sup_{\mathbf{x} \in \Omega_{nl}} |u_0^M(\mathbf{x}) - u_0(\mathbf{x}, T)| \leq C(T)\Delta t$. Since $|u_{nl, \delta}^M(\mathbf{x}) - u_0(\mathbf{x}, T)| \leq |u_{nl, \delta}^M(\mathbf{x}) - u_0^M(\mathbf{x})| + |u_0^M(\mathbf{x}) - u_0(\mathbf{x}, T)|$, it suffices to show that $\sup_{\mathbf{x} \in \Omega_{nl}} |u_{nl, \delta}^M(\mathbf{x}) - u_0^M(\mathbf{x})| \leq C(T)\delta^2$. As shown in the left plot of Figure 3, let $\mathbf{z}_3 \in \partial\Omega$ be a point such that $\tau(\mathbf{z}_3)$ is orthogonal to the bisector of the angle $\angle \mathbf{z}_2 \tilde{\mathbf{z}} \mathbf{z}_1$. Set the barrier function as

$$\phi(\mathbf{x}) := |\text{dist}(\mathbf{x}, \tau(\mathbf{z}_3)) + 1|^2. \quad (3.13)$$

Then it can be shown that

$$\begin{aligned} L_\delta \phi(\mathbf{x}) &\geq C, & \text{for } \mathbf{x} \in \Omega_{nl} \setminus B\Omega_i \\ L_{N\delta} \phi(\mathbf{x}) &\geq C[\delta - s_{\mathbf{x}}]^{3/2} \delta^{-5/2} + C_1 > 0, & \text{for } \mathbf{x} \in B\Omega_i \end{aligned}$$

Taking $G(\mathbf{x}) = L_\delta \phi$ for $\mathbf{x} \in \Omega_{nl} \setminus B\Omega_i$, $G(\mathbf{x}) = L_{N\delta} \phi$ for $\mathbf{x} \in B\Omega_i$ in Lemma 3.5, combining the above bounds with the truncation bounds $|T_\delta|$ provided in Lemma 3.4 we finish the proof. For further details on the bounds, we refer the interested readers to [56]. \square

Remark 2. With the maximum principle 3.2, assuming that the nonlocal solution $u_{nl, \delta}(\mathbf{x}, t)$ has sufficient regularity and employing a q^{th} -order temporal discretization method to the nonlocal problem, then for sufficiently small δ , there exists a constant C independent of δ such that

$$\sup_{\mathbf{x} \in \Omega_{nl}} |u_{nl, \delta}^M(\mathbf{x}) - u_0(\mathbf{x}, T)| \leq C(T)(\Delta t^q + \delta^2).$$

Remark 3. The convergence rate in Theorem 1 is optimal considering the $O(\delta^2)$ convergence of the nonlocal equation to its local limit away from the boundary.

3.2. A Nonlocal Robin-Type and Corner Boundary Condition

Based on the Neumann-type constraint problem, we now develop the nonlocal analog to the classical Robin boundary condition $\beta u(\mathbf{x}) + \frac{\partial u}{\partial \mathbf{n}}(\mathbf{x}) = g(\mathbf{x})$ with $\beta \neq 0$ on a sharp interface Γ_i . Specifically, we propose the nonlocal Robin-type boundary condition with a modified formulation in $B\Omega_i$:

$$\begin{aligned} Q_\delta(\mathbf{x})\dot{u}_{nl,\delta}(\mathbf{x}, t) - 2\alpha_{nl} \int_{\Omega_{nl}} J_\delta(|\mathbf{x} - \mathbf{y}|)(u_{nl,\delta}(\mathbf{y}, t) - u_{nl,\delta}(\mathbf{x}, t))d\mathbf{y} + \alpha_{nl}\beta V_\delta(\mathbf{x})u_{nl,\delta}(\bar{\mathbf{x}}, t) \\ - 2\alpha_{nl}M_\delta(\mathbf{x}) \int_{-\delta}^{\delta} H_\delta(|l|)(u_{nl,\delta}(\mathbf{x}_l, t) - u_{nl,\delta}(\mathbf{x}, t))d\mathbf{x}_l = Q_\delta(\mathbf{x})f_{nl}(\mathbf{x}, t) + \alpha_{nl}V_\delta(\mathbf{x})g(\bar{\mathbf{x}}, t), \end{aligned} \quad (3.14)$$

where $Q_\delta(\mathbf{x})$, $V_\delta(\mathbf{x})$, and $M_\delta(\mathbf{x})$ are as defined in (3.3)-(3.5). We then obtain the following nonlocal constraint problem

$$\begin{aligned} \dot{u}_{nl,\delta}(\mathbf{x}, t) - \alpha_{nl}\mathcal{L}_\delta u_{nl,\delta}(\mathbf{x}, t) &= f_{nl}(\mathbf{x}, t), \quad \mathbf{x} \in \Omega_{nl} \setminus B\Omega_i \\ Q_\delta(\mathbf{x})\dot{u}_{nl,\delta}(\mathbf{x}, t) - \alpha_{nl}\mathcal{L}_{N\delta} u_{nl,\delta}(\mathbf{x}, t) + \alpha_{nl}\beta V_\delta(\mathbf{x})u_{nl,\delta}(\bar{\mathbf{x}}, t) &= Q_\delta(\mathbf{x})f_{nl}(\mathbf{x}, t) + \alpha_{nl}V_\delta(\mathbf{x})g(\bar{\mathbf{x}}, t), \quad \mathbf{x} \in B\Omega_i \\ u_{nl,\delta}(\mathbf{x}, t) &= u_{nl}^D(\mathbf{x}, t), \quad \mathbf{x} \in B\Omega_d \\ u_{nl,\delta}(\mathbf{x}, 0) &= u^{IC}(\mathbf{x}). \quad \mathbf{x} \in \Omega_{nl} \end{aligned} \quad (3.15)$$

Employing the backward Euler scheme for time integration and the meshfree quadrature rule described in Section 2.1, for $\mathbf{x}_i \in B\Omega_i$, we solve for $(U_\delta)_i^k \approx u_{nl,\delta}(\mathbf{x}_i, t^k)$ with:

$$\begin{aligned} \frac{Q_\delta(\mathbf{x}_i)}{\Delta t}((U_\delta)_i^{k+1} - (U_\delta)_i^k) - 2\alpha_{nl}\tilde{u}_\delta^{k+1} DP(P^T DP)^{-1} \int_{B(\mathbf{x}_i, \delta) \cap \Omega_{nl}} J_\delta(|\mathbf{y} - \mathbf{x}_i|)(R(\mathbf{y}) - R(\mathbf{x}_i))d\mathbf{y} \\ - 2\alpha_{nl}\tilde{u}_\delta^{k+1} DP(P^T DP)^{-1} M_\delta(\mathbf{x}_i) \int_{-\delta}^{\delta} H_\delta(|l|)(R(\mathbf{x}_l) - R(\mathbf{x}_i))d\mathbf{x}_l + \alpha_{nl}\beta V_\delta(\mathbf{x}_i)(U_\delta)_i^{k+1} \\ = Q_\delta(\mathbf{x}_i)f_{nl}(\mathbf{x}_i, t^{k+1}) + \alpha_{nl}V_\delta(\mathbf{x}_i)g(\bar{\mathbf{x}}_i, t^{k+1}), \end{aligned} \quad (3.16)$$

with $\tilde{u}_\delta^k = ((U_\delta)_j^k : j \in I(\mathbf{x}_i))^T \in \mathbb{R}^{\#I(\mathbf{x}_i)}$. $(U_\delta)_i^k$ represents the solution corresponding to $\bar{\mathbf{x}}_i$ which may be estimated based on the generalized moving least squares (GMLS) approximation framework if $\bar{\mathbf{x}}_i$ is not in the collection of grid points χ_h .

Remark 4. The statement of the Robin problem requires solution regularity beyond the L^2 -equivalent nonlocal energy space introduced for the Neumann problem, due to the evaluation of $u_{nl,\delta}$ at $\bar{\mathbf{x}}$. However, the proposed Robin problem is only intended for use in the spatially-discretized setting, where this extra regularity is available. In this work, we consider asymptotically-compatible discretizations, and the continuous problem is in fact the local heat equation, although, more generally, one might incorporate additional phenomena (e.g., bond damage in nonlocal elasticity) such that the vanishing-horizon limit of the nonlocal problem does not correspond to a local problem.

Similar as in [56], to investigate how the new Robin-type constraint formulation extrapolates to the setting of Lipschitz domains, we further extend the proposed formulation to boundary Γ_i with corners. As shown in Figure 4,

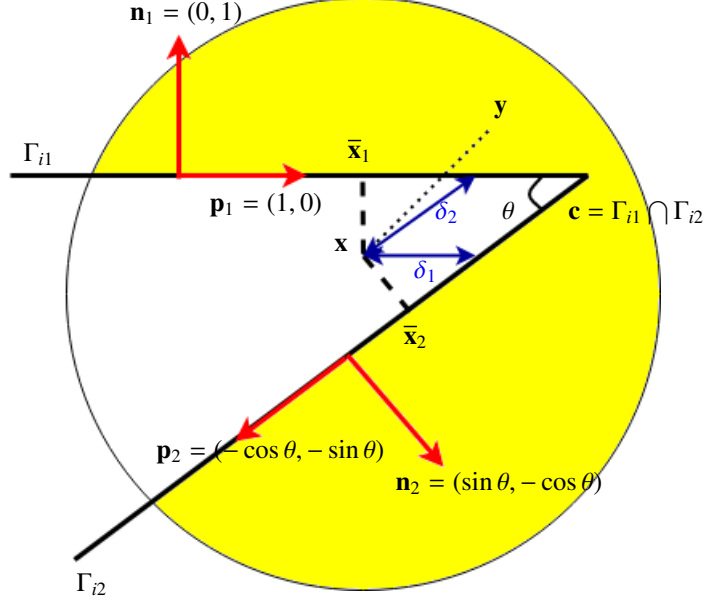


Figure 4: Geometric assumptions and notation for the corner case. Here the yellow region denotes $B(\mathbf{x}, \delta) \cap (\mathbb{R}^2 \setminus \Omega_{nl})$.

here we assume that there are two intersecting boundaries with Robin-type boundary conditions:

$$\beta u + \frac{\partial u}{\partial \mathbf{n}_1} = g_1, \quad \text{on } \Gamma_{i1}, \quad (3.17)$$

$$\beta u + \frac{\partial u}{\partial \mathbf{n}_2} = g_2, \quad \text{on } \Gamma_{i2}, \quad (3.18)$$

and the two boundaries intersect at $\mathbf{c} = \Gamma_{i1} \cap \Gamma_{i2}$. For any point \mathbf{x} satisfying $|\mathbf{x} - \mathbf{c}| < \delta$, we project \mathbf{x} onto the two boundaries respectively, i.e., $\mathbf{x} = \bar{\mathbf{x}}_1 - s_{\mathbf{x}_1} \mathbf{n}_1(\bar{\mathbf{x}}_1) = \bar{\mathbf{x}}_2 - s_{\mathbf{x}_2} \mathbf{n}_2(\bar{\mathbf{x}}_2)$. Here we assume that both Γ_{i1} and Γ_{i2} are straight lines near the corner \mathbf{c} , although the formulation can be further extended to more general cases. Denote θ as the angle between Γ_{i1} and Γ_{i2} , without loss of generality we further denote $\mathbf{n}_1 = (0, 1)$ and $\mathbf{n}_2 = (\sin \theta, -\cos \theta)$. Correspondingly, we have $\mathbf{p}_1 = (1, 0)$ and $\mathbf{p}_2 = (-\cos \theta, -\sin \theta)$. For each point $\mathbf{x} = (x_1, x_2)$, with Taylor expansion we have the following approximation for $u(\mathbf{y}) - u(\mathbf{x})$ with $\mathbf{y} = (y_1, y_2) \in B(\mathbf{x}, \delta) \cap \partial\Omega_{N\delta}$:

$$\begin{aligned} & u(\mathbf{y}, t) - u(\mathbf{x}, t) \\ &= d_1 \frac{\partial u(\mathbf{x}, t)}{\partial \mathbf{n}_1} + d_2 \frac{\partial u(\mathbf{x}, t)}{\partial \mathbf{n}_2} + \frac{1}{2} d_1^2 [u(\mathbf{x}, t)]_{n_1 n_1} + \frac{1}{2} d_2^2 [u(\mathbf{x}, t)]_{n_2 n_2} + d_1 d_2 [u(\mathbf{x}, t)]_{n_1 n_2} + O(\delta^3) \\ &= d_1 [g_1(\bar{\mathbf{x}}_1, t) - \beta u(\bar{\mathbf{x}}_1, t)] + d_2 [g_2(\bar{\mathbf{x}}_2, t) - \beta u(\bar{\mathbf{x}}_2, t)] + \frac{1}{\alpha_{nl}} \left(\frac{1}{2} d_1^2 - (\bar{\mathbf{x}}_1 - \mathbf{x}) \cdot \mathbf{n}_1 d_1 \right) (-f_{nl}(\mathbf{x}, t) - \alpha_{nl} [u(\mathbf{x}, t)]_{p_1 p_1} + \dot{u}(\mathbf{x}, t)) \\ &\quad + \frac{1}{\alpha_{nl}} \left(\frac{1}{2} d_2^2 - (\bar{\mathbf{x}}_2 - \mathbf{x}) \cdot \mathbf{n}_2 d_2 \right) (-f_{nl}(\mathbf{x}, t) - \alpha_{nl} [u(\mathbf{x}, t)]_{p_2 p_2} + \dot{u}(\mathbf{x}, t)) \\ &\quad + \frac{1}{2 \sin \theta} d_1 d_2 \left(\frac{\partial g_1(\bar{\mathbf{x}}_1, t)}{\partial \mathbf{p}_1} - \beta \frac{\partial u(\bar{\mathbf{x}}_1, t)}{\partial \mathbf{p}_1} - \frac{\partial g_2(\bar{\mathbf{x}}_2, t)}{\partial \mathbf{p}_2} + \beta \frac{\partial u(\bar{\mathbf{x}}_2, t)}{\partial \mathbf{p}_2} + \frac{1}{\alpha_{nl}} [f_{nl}(\mathbf{x}, t) - \dot{u}(\mathbf{x}, t)] \sin \theta \cos \theta \right) + O(\delta^3), \end{aligned}$$

where $d_1 := \frac{\cos \theta}{\sin \theta}(y_1 - x_1) + (y_2 - x_2)$, $d_2 := \frac{1}{\sin \theta}(y_1 - x_1)$. Moreover, we have

$$\begin{aligned} [u(\mathbf{x}, t)]_{p_1 p_1} + [u(\mathbf{x}, t)]_{p_2 p_2} &= \frac{1}{\alpha_{nl}} [-f_{nl}(\mathbf{x}, t) + \dot{u}(\mathbf{x}, t)] + \cot \theta \left[\frac{\partial g_1(\bar{\mathbf{x}}_1, t)}{\partial \mathbf{p}_1} - \beta \frac{\partial u(\bar{\mathbf{x}}_1, t)}{\partial \mathbf{p}_1} - \frac{\partial g_2(\bar{\mathbf{x}}_2, t)}{\partial \mathbf{p}_2} + \beta \frac{\partial u(\bar{\mathbf{x}}_2, t)}{\partial \mathbf{p}_2} \right] + O(\delta), \\ \frac{\partial u(\bar{\mathbf{x}}_1, t)}{\partial \mathbf{p}_1} &= \cot \theta g_1(\bar{\mathbf{x}}_1, t) + \frac{1}{\sin \theta} g_2(\bar{\mathbf{x}}_2, t) + O(\delta), \quad \frac{\partial u(\bar{\mathbf{x}}_2, t)}{\partial \mathbf{p}_2} = -\frac{1}{\sin \theta} g_1(\bar{\mathbf{x}}_1, t) - \cot \theta g_2(\bar{\mathbf{x}}_2, t) + O(\delta). \end{aligned}$$

Let

$$D_1 = 2 \int_{\mathbb{R}^2 \setminus \Omega_{nl}} J_\delta(|\mathbf{x} - \mathbf{y}|) \left[\frac{1}{2} d_1^2 - (\bar{\mathbf{x}}_1 - \mathbf{x}) \cdot \mathbf{n}_1 d_1 \right] d\mathbf{y}, \quad D_2 = 2 \int_{\mathbb{R}^2 \setminus \Omega_{nl}} J_\delta(|\mathbf{x} - \mathbf{y}|) \left[\frac{1}{2} d_2^2 - (\bar{\mathbf{x}}_2 - \mathbf{x}) \cdot \mathbf{n}_2 d_2 \right] d\mathbf{y},$$

for $D_1 > D_2$, we take δ_1 as the arc length from \mathbf{x} to Γ_i following the contour parallel to Γ_{i1} and use $2 \int_{-\delta_1}^{\delta_1} H_{\delta_1}(|l|)(u(\mathbf{x}_{l1}, t) - u(\mathbf{x}, t)) d\mathbf{x}_{l1}$ to denote the integral on this contour which approximates $[u(\mathbf{x}, t)]_{p_1 p_1}$. We obtain the following formulation for $\mathbf{x} \in B(\mathbf{c}, \delta) \cap \Omega_{nl}$:

$$\begin{aligned} & Q_\delta^c(\mathbf{x}) \dot{u}_{nl, \delta}(\mathbf{x}, t) - 2\alpha_{nl} \int_{\Omega_{nl}} J_\delta(|\mathbf{x} - \mathbf{y}|) (u_{nl, \delta}(\mathbf{y}, t) - u_{nl, \delta}(\mathbf{x}, t)) d\mathbf{y} + 4\alpha_{nl} (D_1 - D_2) \int_{-\delta_1}^{\delta_1} H_{\delta_1}(|l|) (u_{nl, \delta}(\mathbf{x}_{l1}, t) - u_{nl, \delta}(\mathbf{x}, t)) d\mathbf{x}_{l1} \\ & + 2\alpha_{nl} \beta \int_{\mathbb{R}^2 \setminus \Omega_{nl}} J_\delta(|\mathbf{x} - \mathbf{y}|) \left(d_1 u_{nl, \delta}(\bar{\mathbf{x}}_1, t) + d_2 u_{nl, \delta}(\bar{\mathbf{x}}_2, t) \right) d\mathbf{y} \\ & = Q_\delta^c(\mathbf{x}) f(\mathbf{x}, t) - \alpha_{nl} D_2 \cot \theta \left(\frac{\partial g_1(\bar{\mathbf{x}}_1, t)}{\partial \mathbf{p}_1} - \frac{\partial g_2(\bar{\mathbf{x}}_2, t)}{\partial \mathbf{p}_2} \right) + \beta \alpha_{nl} D_2 \cot \theta \left(\cot \theta + \frac{1}{\sin \theta} \right) (g_1(\bar{\mathbf{x}}_1, t) + g_2(\bar{\mathbf{x}}_2, t)) \\ & + 2\alpha_{nl} \int_{\mathbb{R}^2 \setminus \Omega_{nl}} J_\delta(|\mathbf{x} - \mathbf{y}|) \left(d_1 g_1(\bar{\mathbf{x}}_1, t) + d_2 g_2(\bar{\mathbf{x}}_2, t) + \frac{d_1 d_2}{2 \sin \theta} \left(\frac{\partial g_1(\bar{\mathbf{x}}_1, t)}{\partial \mathbf{p}_1} - \frac{\partial g_2(\bar{\mathbf{x}}_2, t)}{\partial \mathbf{p}_2} \right) \right. \\ & \left. - \beta \frac{d_1 d_2}{2 \sin \theta} \cot \theta \left(\cot \theta + \frac{1}{\sin \theta} \right) (g_1(\bar{\mathbf{x}}_1, t) + g_2(\bar{\mathbf{x}}_2, t)) \right) d\mathbf{y} \end{aligned} \quad (3.19)$$

where

$$Q_\delta^c(\mathbf{x}) = 1 - D_1 + \int_{\mathbb{R}^2 \setminus \Omega_{nl}} J_\delta(|\mathbf{x} - \mathbf{y}|) d_1 d_2 \cos \theta d\mathbf{y}.$$

Else, we take δ_2 as the arc length from \mathbf{x} to Γ_i following the contour parallel to Γ_{i2} and use $2 \int_{-\delta_2}^{\delta_2} H_{\delta_2}(|l|)(u(\mathbf{x}_{l2}, t) - u(\mathbf{x}, t)) d\mathbf{x}_{l2}$ to denote the integral on this contour which approximates $[u(\mathbf{x}, t)]_{p_2 p_2}$. A similar formulation is obtained.

Remark 5. When the domain is concave and $\theta > \pi$ on the corner, it is possible that the projection points $\bar{\mathbf{x}}_1$ and $\bar{\mathbf{x}}_2$ are on the extended lines of Γ_{i1} and Γ_{i2} . In this case, we project \mathbf{x} onto the corner point \mathbf{c} and evaluate g_1, g_2 on \mathbf{c} . The derivation is very similar as above.

3.3. Numerical Results for Nonlocal Boundary Conditions

In this Section, we present numerical tests of the proposed nonlocal boundary treatment on Γ_i , by considering three types of representative domains Ω_{nl} : a square domain in Section 3.3.1 which represents the case with 0 curvature on Γ_i ; a circular domain in Section 3.3.2, which represents a case with nonzero curvature on Γ_i ; and a cross-shape domain

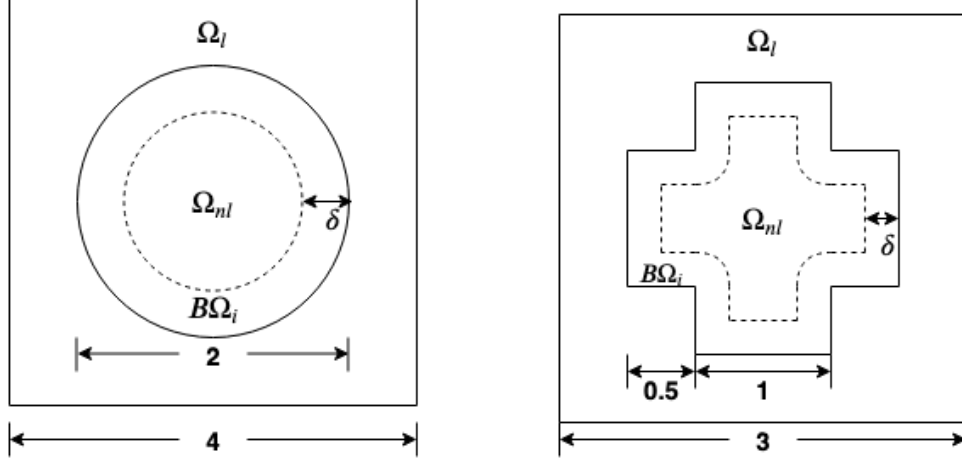


Figure 5: Illustration of the domains employed in numerical tests. Left: problem with a circular nonlocal subdomain and a surrounding local subdomain, corresponding to test 2 in Sections 3.3.2 and 4.3.2. Right: test with a cross-shape nonlocal subdomain and a surrounding local subdomain, corresponding to test 3 in Sections 3.3.2 and 4.3.2.

in Section 3.3.3 which is a non-convex domain with corners and therefore it is outside the scope of the model problem analysis presented earlier in Section 3.1. Illustration of the square domain can be found in the left plot of Figure 2, while the circular domain and the cross-shape domain are shown as the Ω_{nl} region in Figure 5. With the tests we aim to investigate the performance of the proposed nonlocal Neumann and Robin-type constraint formulation on patch tests, and to demonstrate the asymptotic convergence of the meshfree quadrature rule (2.9). To maintain an easily scalable implementation, it is often desirable that the ratio $C_1 \leq \frac{\delta}{h} \leq C_2$ as $\delta \rightarrow 0$. This so-called “M-convergence” results in a sparse linear system with bounded bandwidth that may be solved efficiently with standard preconditioning techniques [44]. Therefore, in the asymptotic compatibility tests we focus on the case with $\delta/h = C$. For simplicity, we set $\alpha_{nl} = 1$ in this section. Although the discussions and the proposed formulations in this paper are not tied to a specific kernel, in numerical tests we demonstrate the numerical performances with $J_\delta(r) = J_\delta^1(r)$.

3.3.1. Test 1: a square domain with a straight line boundary

We first consider the nonlocal heat problem when $\Gamma_i = \{(1, y) | y \in [0, 1]\}$, $\Omega_{nl} = [0, 1] \times [0, 1]$. Dirichlet-type boundary condition are imposed on the other three sides of Ω_{nl} in a collar with width δ . An illustration of the domain can be found in the left plot of Figure 2.

We first demonstrate the asymptotic compatibility. In this test, we set the initial condition $u^{IC} = 0$ and external loading $f^{nl}(x, y, t) = (2t + 2t^2) \sin(x) \cos(y)$. On $B\Omega_d$, a Dirichlet-type boundary condition $u_{nl}^D(x, y, t) := t^2 \sin(x) \cos(y)$ is applied, and a Robin-type boundary condition $g(x, y, t) = \beta t^2 \sin(1) \cos(y) + \pi \cos(1) \cos(y)$ is applied on the sharp interface Γ_i . Here we note that when $\beta = 0$, the Robin-type boundary condition is equivalent to the Neumann-type boundary condition. The local limit of this problem has an analytical solution $u_0(x, y, t) = t^2 \sin(x) \cos(y)$. To investigate the asymptotic compatibility when $\delta/h = C$, we refine δ and h simultaneously keeping the ratio $\delta/h = 3.9$. For time discretization, we integrate until $T = 1$ using the backward-Euler method and $\Delta t = 100h^2$. The convergence

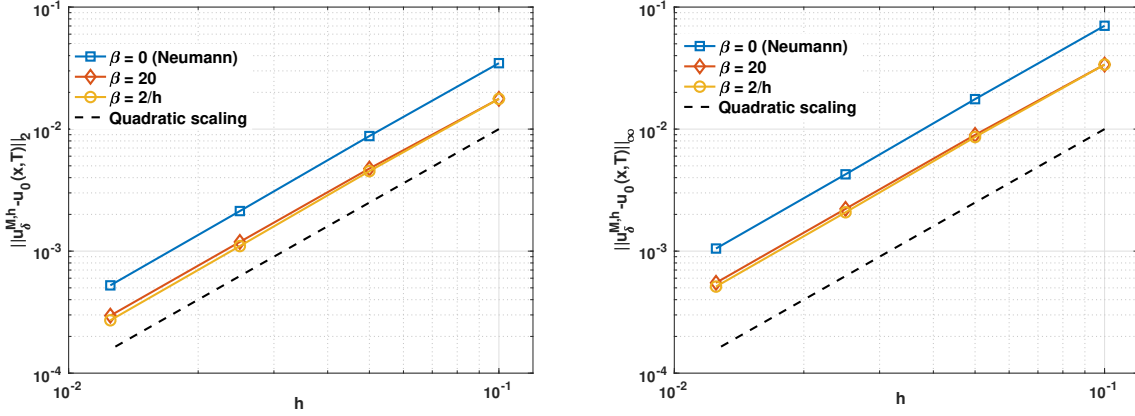


Figure 6: Test 1 results for nonlocal boundary condition on a square domain. Left: convergence of the numerical nonlocal solution to the local limit with different Robin coefficients, in the L^2 norm. Right: convergence of the numerical nonlocal solution to the local limit with different Robin coefficients, in the L^∞ norm.

results are presented in Figure 6, where we demonstrate the difference between the numerical nonlocal solution and the analytical local limit $\|u_{nl,\delta}^{M,h} - u_0(\mathbf{x}, T)\|$. Three different sets of Robin coefficients are employed here: (1) $\beta = 0$ which is equivalent to the Neumann-type boundary condition; (2) β is a non-zero constant, and (3) $\beta = C/h$. Note that the case (3) is tested here since $\beta = C/h$ is the most robust Robin coefficient for local-to-nonlocal coupling framework, as will be further discussed in Section 4. It is observed from Figure 6 that the second-order convergence $O(\delta^2)$ is achieved from all three sets of Robin coefficients, which therefore verifies the analysis in Section 3.1 for the Neumann-type boundary condition and demonstrates the asymptotic compatibility of the numerical solver. The results on cases (2) and (3) illustrate that the second order convergence $O(\delta^2)$ is also achieved on the nonlocal problem with Robin-type boundary condition, which can be seen as a generalization of the nonlocal Neumann-type boundary condition.

Moreover, we investigate the linear patch test problem with analytical linear solution $u_{nl} = u_0 = x$ and the quadratic patch test problem with analytical quadratic solution $u_{nl} = u_0 = x^2$. In the absence of forcing terms and with consistent boundary conditions on $B\Omega_d$ and Γ_i , we investigate if the nonlocal Robin-type constraint problem returns the accurate analytical nonlocal solution. The numerical results along the domain center line $y = 1/2$ are reported in Figure 7. We observe that the numerical solution from the proposed Robin-type boundary condition passes both the linear and quadratic patch tests within machine precision accuracy and for several values of h and β .

3.3.2. Test 2: a circular domain

We now consider a domain which has boundaries with non-zero curvature. As shown in the left side of Figure 5, we employ $\Omega_{nl} = \{(x, y) | x^2 + y^2 \leq 1\}$ and $\Gamma_i = \partial\Omega_{nl} \setminus \{(0, -1)\}$, with a similar problem setting for initial condition and external loading as in test 1, namely, $u^{IC} = 0$ and $f^{nl}(x, y, t) = (2t + 2t^2) \sin(x) \cos(y)$. A Robin-type boundary condition $g(x, y, t) = \beta t^2 \sin(x) \cos(y) + t^2(x \cos(x) \cos(y) - y \sin(x) \sin(y))$ is applied on the sharp interface Γ_i . To make the problem well-posed in the $\beta = 0$ case, we set $u_{nl}^D(x, y, t) := t^2 \sin(x) \cos(y)$ on $(x, y) = (0, -1)$. Similarly as in test

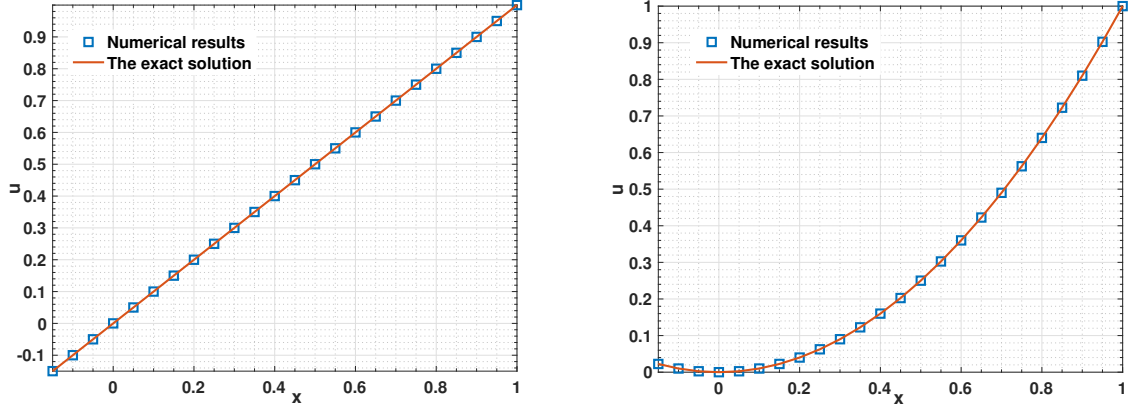


Figure 7: Test 1 results for nonlocal boundary condition on a square domain. Left: linear patch test. The comparison of numerical results with $h = 1/20$, $\beta = 10$ and the analytical solution $u = x$. Right: quadratic patch test. The comparison of numerical results with $h = 1/20$, $\beta = 10$ and the analytical solution $u = x^2$.

1, this problem setting has an analytical local limit $u_0(x, y, t) = t^2 \sin(x) \cos(y)$. Considering $\delta/h = 3.9$, $\Delta t = 100h^2$ while decreasing the spatial discretization size h , the comparison of numerical nonlocal solution and the analytical local limit u_0 at $T = 1$ are presented in Figure 8, again with three sets of Robin coefficients: (1) $\beta = 0$; (2) β is a non-zero constant; and (3) $\beta = C/h$. It can be observed that with all three sets of Robin-coefficients we have achieved $O(\delta^2)$ convergence rate to the corresponding local limit. Therefore, the proposed Robin-type boundary formulation is asymptotically compatible with boundaries that have a non-zero curvature and $\delta/h = C$.

3.3.3. Test 3: a cross-shape domain

We now consider a more complicated domain which doesn't satisfy the convex and C^3 regularity requirements in the convergence analysis of Section 3.1. The domain is of cross-shape, presented as Ω_{nl} in the right plot of Figure 5. Neumann or Robin-type boundary conditions are applied everywhere over the boundary except on point $(-1, -0.5)$ where we set $u_{nl}^D(x, y, t) = t^2 \sin(x) \cos(y)$, in order to make the problem well-posed on $\beta = 0$ case. Note that this domain is non-convex and the boundary include corners. Therefore, for $\mathbf{x} \in B\Omega_i$ within distance δ to the corner, we employ the corner formulation developed in (3.19). In this test we set $u^{IC} = 0$, $f^{nl}(x, y, t) = (2t + 2t^2) \sin(x) \cos(y)$ and a Robin-type boundary condition $g(x, y, t) = \beta t^2 \sin(x) \cos(y) + t^2 (\cos(x) \cos(y) n_x - \sin(x) \sin(y) n_y)$ is applied on the sharp interface Γ_i , where $\mathbf{n} = (n_x, n_y)$ is the outward-pointing unit normal vector on Γ_i . The analytical local limit solution for above problem setting is also $u_0(x, y, t) = t^2 \sin(x) \cos(y)$. Keep a fixed ratio $\delta/h = 3.5$, $\Delta t = 100h^2$ while refining the spatial discretization length scale h , the L^2 and L^∞ norm for the difference between numerical nonlocal solution and the analytical local limit at $T = 1$ are presented in Figure 9, from which a second-order convergence rate $O(\delta^2)$ is observed. This example verifies the proposed corner formulation and illustrates that the proposed nonlocal Robin-type formulation also achieves asymptotic compatibility on a non-convex domain consisting of line segments and corners, which greatly improves the applicability of the proposed formulation for more complicated scenarios.

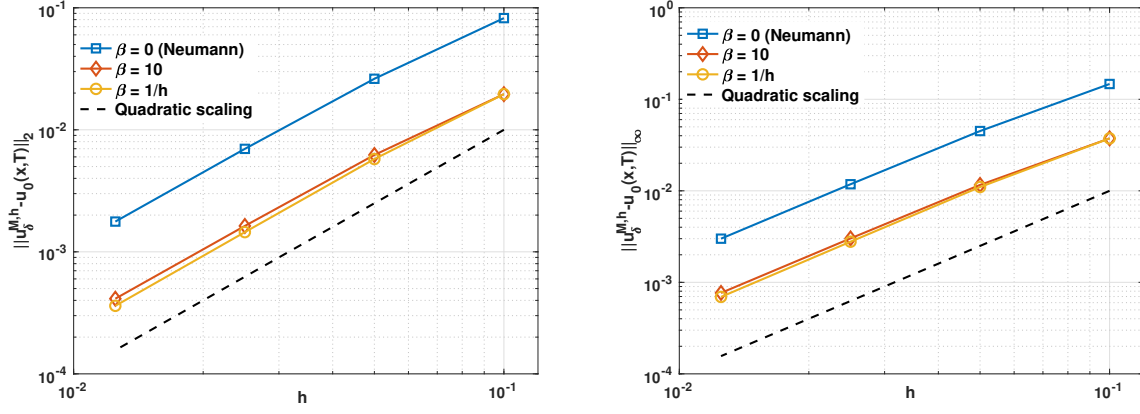


Figure 8: Test 2 results for nonlocal boundary condition on a circular domain. Left: convergence of the numerical nonlocal solution to the local limit with different Robin coefficients, in the L^2 norm. Right: convergence of the numerical nonlocal solution to the local limit with different Robin coefficients, in the L^∞ norm.

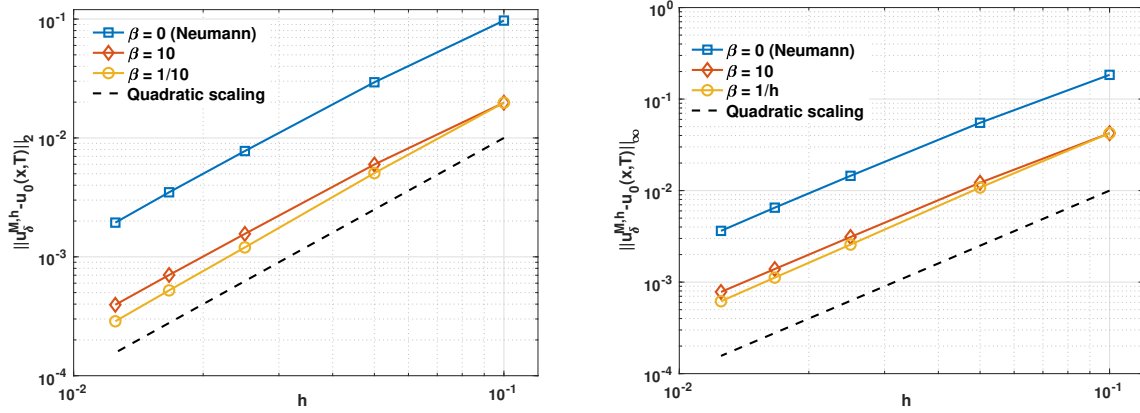


Figure 9: Test 3 results for nonlocal boundary condition on a cross-shape domain. Left: convergence of the numerical nonlocal solution to the local limit with different Robin coefficients, in the L^2 norm. Right: convergence of the numerical nonlocal solution to the local limit with different Robin coefficients, in the L^∞ norm.

4. Nonoverlapping Local-to-Nonlocal (LtN) Coupling Framework

In this section, we present an explicit coupling procedure for the local-to-nonlocal coupling problem without overlapping regions. In this coupling framework, a partitioned procedure is employed such that the nonlocal and local subproblems are solved separately, which allows for the reuse of existing codes/methods. This is of particular value in the case of local-to-nonlocal coupling, since the different model classes are often solved with radically-different code architectures (although similarities have recently been pointed out between certain meshfree discretizations of local and nonlocal problems [69]). The local and nonlocal solvers exchange transmission conditions on the sharp interface Γ_i , to enforce the continuity of solutions and the energy balance of the whole system. The partitioned procedure can be broadly classified as either explicit or implicit (see, e.g., [57, 70–73]). In explicit coupling strategies, the solution of each sub-problem and the exchange of interface data are performed only once (or a few times) per time step, while in the implicit coupling strategies an additional sub-iteration is employed at each time step and each sub-problem is solved in a partitioned way via sub-iterations until convergence. For dynamic problems, the explicit coupling strategy is generally more efficient than the implicit coupling strategy, although the former is more likely to be unstable. To develop a stable explicit coupling strategy, proper transmission conditions are required. In the current paper we propose to employ the Robin-type transmission condition, which was proven to be effective in stabilizing the explicit coupling strategy on domain decomposition problems [74, 75]. Specifically, for the nonlocal subproblem, we solve for the nonlocal heat equation (3.15) with the Robin-type boundary condition applied on the interface Γ_i . For the local subproblem, we solve a classical heat equation (2.10) with the classical Dirichlet boundary condition applied on the interface Γ_i . To improve the stability and efficiency of the coupling framework, we propose a numerical approach to choose the Robin coefficient β .

This section is organized as follows: In Section 4.1, we present an explicit coupling procedure for the proposed local-to-nonlocal coupling approach, then in Section 4.2 we introduce an approach to numerically obtain the optimal Robin coefficient by minimizing the amplification factor in the discretized coupling system; To numerically verify the proposed local-to-nonlocal coupling approach, in Section 4.3, we investigate its performance on three different numerical tests with various configuration settings.

4.1. An Explicit Coupling Approach with Robin Transmission Conditions

In this section, we propose an explicit nonoverlapping local-to-nonlocal coupling framework, by employing the Robin transmission condition developed in Section 3. Note that here we present the nonlocal model for the case without corners only, since for the case with corners one can simply replace the nonlocal formulation (3.14) with (3.19).

To introduce the partitioned procedure, we consider a semi-discretized system where the backward Euler method is employed for time discretization. At time step k , we solve for the nonlocal solution $u_{nl,\delta}^k$ in Ω_{nl} and the local solution

u_l^k in Ω_l using the solutions at the previous time step, $u_{nl,\delta}^{k-1}$ and u_l^{k-1} : we first solve for $u_{nl,\delta}^k$ with

$$\frac{1}{\Delta t}(u_{nl,\delta}^k(\mathbf{x}) - u_{nl,\delta}^{k-1}(\mathbf{x})) - \alpha_{nl}\mathcal{L}_\delta u_{nl,\delta}^k(\mathbf{x}) = f_{nl}(\mathbf{x}, t^k), \quad \mathbf{x} \in \Omega_{nl} \setminus B\Omega_i \quad (4.1a)$$

$$\begin{aligned} & \frac{1}{\Delta t}Q_\delta(\mathbf{x})(u_{nl,\delta}^k(\mathbf{x}) - u_{nl,\delta}^{k-1}(\mathbf{x})) - \alpha_{nl}\mathcal{L}_{N\delta}u_{nl,\delta}^k(\mathbf{x}) + \alpha_{nl}\beta V_\delta(\mathbf{x})u_{nl,\delta}^k(\bar{\mathbf{x}}) \\ & = Q_\delta(\mathbf{x})f_{nl}(\mathbf{x}, t^k) + \alpha_{nl}V_\delta(\mathbf{x})\left[\frac{\partial u_l^{k-1}(\bar{\mathbf{x}})}{\partial \mathbf{n}} + \beta u_l^{k-1}(\bar{\mathbf{x}})\right], \quad \mathbf{x} \in B\Omega_i \end{aligned} \quad (4.1b)$$

$$u_{nl,\delta}^k(\mathbf{x}) = u_{nl}^D(\mathbf{x}, t^k), \quad \mathbf{x} \in B\Omega_d \quad (4.1c)$$

then solve for u_l^k with

$$\frac{1}{\Delta t}(u_l^k(\mathbf{x}) - u_l^{k-1}(\mathbf{x})) - \alpha_l\Delta u_l^k(\mathbf{x}) = f_l(\mathbf{x}, t^k), \quad \mathbf{x} \in \Omega_l \quad (4.2a)$$

$$u_l^k(\mathbf{x}) = u_{nl,\delta}^k(\mathbf{x}), \quad \mathbf{x} \in \Gamma_i \quad (4.2b)$$

$$u_l^k(\mathbf{x}) = u_l^D(\mathbf{x}, t^k). \quad \mathbf{x} \in \Gamma_d \quad (4.2c)$$

Here β is the Robin coefficient which is to be determined in Section 4.2 to achieve the optimal coupling performance. \mathbf{n} is the normal vector on interface Γ_i pointing from the nonlocal subdomain to the local subdomain. Q_δ, V_δ are functions depending on the position of \mathbf{x} and the nonlocal domain geometry, with formulations given in (3.3)-(3.4). The nonlocal operator $\mathcal{L}_{N\delta}$ for $\mathbf{x} \in B\Omega_i$ is defined in (3.6). In this coupling problem we employ Dirichlet transmission conditions for the local problem and nonlocal Neumann or Robin transmission conditions for the nonlocal problem on the sharp local-nonlocal coupling interface Γ_i . For presentation simplicity, in the following we neglect the Dirichlet boundary conditions on $B\Omega_d$ and Γ_d when presenting the fully-discretized formulation, and focus on the interface transmission conditions.

In the coupling formulation introduced in (4.1)-(4.2), since different solvers are employed for the two sub-problems, the local and nonlocal grid points on Γ_i is possibly non-conforming. Therefore, to impose the interface transmission conditions one can not simply pass the nodal values on the interface between the local and nonlocal solvers. To obtain the nonlocal Robin-type interface condition, for $\mathbf{x}_j \in \chi_h \cap B\Omega_i$ we approximate the Robin condition on its projection of Γ_i as the interpolation with the solution on local nodes. Denoting $\mathbf{U}_{nl,B\Omega_i}$ as the vector of nodal values of the nonlocal solution when $\mathbf{x}_j \in \chi_h \cap B\Omega_i$, $\mathbf{U}_{nl,in}$ as the vector of the nonlocal solution on nodes $\mathbf{x}_j \in \chi_h \cap (\Omega_{nl} \setminus B\Omega_i)$, \mathbf{U}_{l,Γ_i} as the vector of nodal values of the local solution on interface Γ_i and $\mathbf{U}_{l,in}$ as the vector of nodal values of the local solution on the interior nodes, for each $\mathbf{x}_j \in \chi_h \cap B\Omega_i$ we obtain $g(\bar{\mathbf{x}}_j)$ from nodal values of the numerical local solution:

$$\frac{\partial u_l^{k-1}(\bar{\mathbf{x}}_j)}{\partial \mathbf{n}} + \beta u_l^{k-1}(\bar{\mathbf{x}}_j) \approx [T_1 \mathbf{U}_{l,in}^{k-1} + T_2 \mathbf{U}_{l,\Gamma_i}^{k-1}]_j. \quad (4.3)$$

Note here T_1 and T_2 are matrices formed by interpolation coefficients, and their elements linearly depend on the Robin

coefficient β . With the above interpolation formulation, we can then substitute the Robin transmission condition $\frac{\partial u_l^{k-1}(\bar{\mathbf{x}})}{\partial \mathbf{n}} + \beta u_l^{k-1}(\bar{\mathbf{x}})$ applied on the sharp interface Γ_i into (3.14), and formulate the fully discretized nonlocal subproblem as the following linear system:

$$\begin{aligned} \frac{M_{nl,in}}{\Delta t} \mathbf{U}_{nl,in}^k + A_{11} \mathbf{U}_{nl,in}^k + A_{12} \mathbf{U}_{nl,B\Omega_i}^k &= \mathbf{F}_{nl,in}^k + \frac{M_{nl,in}}{\Delta t} \mathbf{U}_{nl,in}^{k-1}, \\ \frac{M_{nl,B\Omega_i}}{\Delta t} \mathbf{U}_{nl,B\Omega_i}^k + A_{21} \mathbf{U}_{nl,in}^k + A_{22} \mathbf{U}_{nl,B\Omega_i}^k + \beta \Sigma_1 \mathbf{U}_{nl,B\Omega_i}^k &= \mathbf{F}_{nl,B\Omega_i}^k + \frac{M_{nl,B\Omega_i}}{\Delta t} \mathbf{U}_{nl,B\Omega_i}^{k-1} + \Sigma_1 T_1 \mathbf{U}_{l,in}^{k-1} + \Sigma_1 T_2 \mathbf{U}_{l,\Gamma_i}^{k-1}. \end{aligned} \quad (4.4)$$

Here $M_{nl,in}$, $M_{nl,B\Omega_i}$ are the mass matrices corresponding to the nodes in $\Omega_{nl} \setminus B\Omega_i$ and in $B\Omega_i$, respectively, $\mathbf{F}_{nl,in}^k$ and $\mathbf{F}_{nl,B\Omega_i}^k$ are the external loading terms for nodes in $\Omega_{nl} \setminus B\Omega_i$ and in $B\Omega_i$, respectively, A_{ij} , $i, j \in \{1, 2\}$, are parts of the stiffness matrices, and Σ_1 handles the $V_\delta(\mathbf{x})$ term and the mapping of each $\bar{\mathbf{x}}_i$ onto the vector $\mathbf{U}_{nl,B\Omega_i}$. On the other hand, to apply the Dirichlet boundary condition on the local side, we need to interpolate the nonlocal numerical solution \mathbf{U}_{nl}^k to obtain an approximation for each $u_{nl,\delta}^k(\mathbf{x}_j)$ where $\mathbf{x}_j \in \Gamma_i$ is a node in the local subdomain mesh. Employing the moving least square method [61, 76] with support radius of size δ and quadratic basis, we reconstruct $u_{nl,\delta}^k(\mathbf{x}_j)$ as a linear combination from nodal values of the nonlocal solution in $B\Omega_i$:

$$u_{nl,\delta}^k(\mathbf{x}_j) \approx \left[\Sigma_2 \mathbf{U}_{nl,B\Omega_i}^k \right]_j. \quad (4.5)$$

Substituting the Dirichlet transmission condition into the local subproblem (2.12), we then obtain a linear system for the fully discretized local subproblem:

$$\begin{aligned} \frac{M_l}{\Delta t} \mathbf{U}_{l,in}^k + B_{11} \mathbf{U}_{l,in}^k + B_{12} \mathbf{U}_{l,\Gamma_i}^k &= \mathbf{F}_l^k + \frac{M_l}{\Delta t} \mathbf{U}_{l,in}^{k-1}, \\ \mathbf{U}_{l,\Gamma_i}^k &= \Sigma_2 \mathbf{U}_{nl,B\Omega_i}^k. \end{aligned} \quad (4.6)$$

Here M_l is the local mass matrix, \mathbf{F}_l is the global vector of the external loads, and B_{11} , B_{12} together forms the local stiffness matrix $[B_{11}, B_{12}] = B_l$.

In summary, we obtain the following fully-discretized explicit local-to-nonlocal coupling algorithm:

1. (Both Solvers): Set initial values for \mathbf{U}_{nl}^0 and \mathbf{U}_l^0 with the given initial condition $u^{IC}(\mathbf{x})$.
2. for $k = 1, \dots, M = T/\Delta t$, do
 - (a) (Local Solver): Calculate the nonlocal transmission condition from the local solution \mathbf{U}_l^{k-1} by perform interpolation for each $\mathbf{x}_j \in \chi_h \cap B\Omega_i$ via (4.3). Pass the results to the nonlocal solver.
 - (b) (Nonlocal Solver): Solve the linear system (4.4) of the nonlocal subproblem for the vector of nodal values of the nonlocal solution $\mathbf{U}_{nl,in}^k$ and $\mathbf{U}_{nl,B\Omega_i}^k$.
 - (c) (Nonlocal Solver): Calculate the local transmission condition from the nonlocal solution $\mathbf{U}_{nl,B\Omega_i}^k$ via the interpolation formulation in (4.5). Pass the results to the local solver.

- (d) (Local Solver): Solve the linear system (4.6) of the local subproblem for the vector of nodal values of the local solution $\mathbf{U}_{l,in}^k$ and $\mathbf{U}_{l,\Gamma_i}^k$.
- (e) Go to time step $k + 1$.

4.2. Estimates for the Optimal Robin Coefficient

As will be observed from the numerical tests in Section 4.3, the explicit coupling strategy may suffer from slow convergence or even divergence, and therefore a good choice of the Robin coefficient is a necessity. The optimal Robin coefficients can be estimated either theoretically or numerically. In problems with relatively simple and/or structured domain settings, one can perform Fourier decomposition to the analytical solution and obtain the optimal Robin coefficient by minimizing the analytic reduction factor, as shown in [40]. However, for the coupling problem with general geometry, deriving the analytic expression of the optimal Robin coefficient is often not straightforward, and therefore in this paper we propose a numerical approach to approximate the optimal Robin coefficient β .

To perform a stability analysis, we consider the homogeneous local-to-nonlocal coupling problem. At the k -th time step, the fully discretized coupling system is written as

$$\begin{bmatrix} \frac{M_{nl,in}}{\Delta t} + A_{11} & A_{12} & 0 & 0 \\ A_{21} & \frac{M_{nl,B\Omega_i}}{\Delta t} + A_{22} + \beta\Sigma_1 & 0 & 0 \\ 0 & 0 & \frac{M_l}{\Delta t} + B_{11} & B_{12} \\ 0 & -\Sigma_2 & 0 & I \end{bmatrix} \begin{bmatrix} \mathbf{U}_{nl,in}^k \\ \mathbf{U}_{nl,B\Omega_i}^k \\ \mathbf{U}_{l,in}^k \\ \mathbf{U}_{l,\Gamma_i}^k \end{bmatrix} = \begin{bmatrix} \frac{M_{nl,in}}{\Delta t} & 0 & 0 & 0 \\ 0 & \frac{M_{nl,B\Omega_i}}{\Delta t} & \Sigma_1 T_1 & \Sigma_1 T_2 \\ 0 & 0 & \frac{M_l}{\Delta t} & 0 \\ 0 & 0 & 0 & 0 \end{bmatrix} \begin{bmatrix} \mathbf{U}_{nl,in}^{k-1} \\ \mathbf{U}_{nl,B\Omega_i}^{k-1} \\ \mathbf{U}_{l,in}^{k-1} \\ \mathbf{U}_{l,\Gamma_i}^{k-1} \end{bmatrix}.$$

Here the first row corresponds to the discretized nonlocal equation of the interior region, the second row represents the modified nonlocal formulation in $B\Omega_i$ with the nonlocal Robin-type transmission condition, the third row corresponds to the discretized local equation of the interior local nodes, and the last row applies the Dirichlet transmission condition at the interface on the local side. Denoting the matrix Λ as

$$\Lambda = \begin{bmatrix} \frac{M_{nl,in}}{\Delta t} + A_{11} & A_{12} & 0 & 0 \\ A_{21} & \frac{M_{nl,B\Omega_i}}{\Delta t} + A_{22} + \beta\Sigma_1 & 0 & 0 \\ 0 & 0 & \frac{M_l}{\Delta t} + B_{11} & B_{12} \\ 0 & -\Sigma_2 & 0 & I \end{bmatrix}^{-1} \begin{bmatrix} \frac{M_{nl,in}}{\Delta t} & 0 & 0 & 0 \\ 0 & \frac{M_{nl,B\Omega_i}}{\Delta t} & \Sigma_1 T_1 & \Sigma_1 T_2 \\ 0 & 0 & \frac{M_l}{\Delta t} & 0 \\ 0 & 0 & 0 & 0 \end{bmatrix}, \quad (4.7)$$

and $\{\lambda_i\}$ as the eigenvalues of the matrix Λ , in the homogeneous coupling system the magnitude of λ_i characterizes the convergence rate of the error component along the i -th eigenvector, and the fully discretized coupling system is stable when the magnitudes of all λ_i are bounded by 1. Therefore, we define an amplification factor as $\max_i |\lambda_i|$, then

numerically obtain the optimal Robin coefficient β by minimizing the reduction factor:

$$\beta = \arg \min_{\beta \geq 0} \left(\max_i |\lambda_i(\tilde{\beta})| \right). \quad (4.8)$$

Remark 6. The expression of Λ in (4.7) indicates that the optimal Robin coefficient may depend on the local and nonlocal subdomains, the time step size Δt , the local and nonlocal discretization methods and the spatial discretization length scale h , and the diffusivity parameters α_l and α_{nl} . For systems with large degree of freedoms, the matrix Λ is of size $(DOF_{nl} + DOF_l)^2$ which might make the calculation of eigenvalues unfeasible. However, two observations make the proposed numerical approach applicable for large local-to-nonlocal coupling systems:

- The matrix Λ is independent of time and therefore the analysis on amplification factor only needs to be performed once.
- In numerical tests of Section 4.3, we have observed that when taking the CFL-like condition $\Delta t = O(h^2)$ the optimal Robin coefficient β scales with the spatial discretization length scale h as $\beta = O(1/h)$. This finding was also suggested in literatures on applying Robin transmission conditions in other domain-decomposition problems, such as in fluid–structure interaction problems (see, e.g., [74]).

Therefore, for a dynamic local-to-nonlocal coupling problem, one only need to calculate the optimal Robin coefficient β_0 once on a coarse grid with spatial discretization length scale h_0 with the same domain settings. A scaled Robin coefficient $\beta = \frac{\beta_0 h_0}{h}$ can then be employed in the final simulation with spatial discretization length scale h .

Remark 7. In the explicit coupling strategy (4.1)-(4.2), since the transmission condition $\left[\frac{\partial u_l^{k-1}(\bar{\mathbf{x}})}{\partial \mathbf{n}} + \beta u_l^{k-1}(\bar{\mathbf{x}}) \right]$ from the local side is generated by the local solution from the last time step, the Robin-type transmission condition (4.1b) results in a splitting error. When employing the Robin coefficient $\beta = O(1/h)$ and considering piecewise linear finite elements in the explicit coupling strategy of two classical local heat equations, this splitting error was reported to be of order $\frac{\Delta t}{h}$ (see, e.g., [74, 77]) in L^2 error estimates. Therefore, the time step Δt has to be chosen small enough compared to the spatial discretization size h . For instance, under a “CFL-like” condition $\Delta t = O(h^2)$ the splitting error is expected to be of order $O(h)$.

4.3. Numerical Results for Local-to-Nonlocal Coupling Framework

In this section, we present a series of numerical tests using the proposed local-to-nonlocal coupling framework, where the nonlocal subdomain is either adjacent to the local subdomain (as shown in the left plot of Figure 1) or embedded in the local subdomain (as shown in the right plot of Figure 1). Specifically, three types of representative domain decomposition settings are employed: (1) In Section 4.3.1, we consider a square nonlocal subdomain which is adjacent to a square local subdomain on one side. The coupling configuration is illustrated in the left plot of Figure 1. (2) In Section 4.3.2, we demonstrate the case with a circular nonlocal subdomain fully embedded in a square

local subdomain, as shown in the left plot of Figure 5. (3) To investigate the coupling framework performance on complicated domain settings we consider a cross-shape nonlocal subdomain embedded in a square local subdomain in Section 4.3.3. An illustration of the settings is shown in the right plot of Figure 5. With these tests, we aim to provide a validation for our analysis of the optimal Robin coefficient β , and to demonstrate the capability of our coupling framework in handling both homogeneous ($\alpha_l = \alpha_{nl}$) and heterogeneous ($\alpha_l \neq \alpha_{nl}$) local-to-nonlocal coupling systems with non-trivial domain configuration settings. Moreover, to demonstrate the asymptotic convergence of the propose coupling approach when the nonlocal interaction region $\delta \rightarrow 0$, in this section we also demonstrate the “M-convergence” of the coupling framework by fixing the ratio of δ and the spatial discretization length h and take $h \rightarrow 0$. As discussed in Remark 7, to provide an $O(h)$ bound for the splitting error introduced in the explicit coupling strategy, in all tests we choose the time step size Δt following a “CFL-like” condition $\Delta t = O(h^2)$.

4.3.1. LtN Test 1: coupling problem with a straight line interface

As the first local-to-nonlocal coupling (LtN) test, we consider a local-to-nonlocal coupling problem where the local and nonlocal subdomains are adjacent, as demonstrated in the left plot of Figure 1. Specifically, in this test we set $\Omega_{nl} = [0, 1] \times [0, 1]$, $\Omega_l = [1, 2] \times [0, 1]$ and demonstrate the numerical performance of the coupling framework on both $\alpha_l = \alpha_{nl}$ and $\alpha_l \neq \alpha_{nl}$ cases. For each case we first investigate the optimal Robin coefficient β following the numerical approach introduced in (4.8), then employ the optimal β to study the asymptotic convergence of the numerical solution to the local limit when $\Delta t, \delta, h \rightarrow 0$. We also employ linear/quadratic analytical solutions on both subdomains to investigate the patch-test consistency of the proposed coupling method.

We first consider the $\alpha_l = \alpha_{nl}$ case by assuming $\alpha_l = \alpha_{nl} = 1$, without loss of generality. In this test, the initial temperature $u^{IC} = 0$ in the whole domain. In the nonlocal exterior boundary $B\Omega_d$ and the local exterior boundary Γ_d , prescribed Dirichlet boundary conditions

$$u_{nl}^D(x, y, t) = t \sin(x) \cos(y), \quad u_l^D(x, y, t) = t \sin(x) \cos(y), \quad (4.9)$$

are applied. The external loadings are set as

$$f_{nl}(x, y, t) = (1 + 2t) \sin(x) \cos(y), \text{ for } (x, y) \in \Omega_{nl}, \quad f_l(x, y, t) = (1 + 2t) \sin(x) \cos(y), \text{ for } (x, y) \in \Omega_l. \quad (4.10)$$

This problem has the following analytical solution for the local subproblem:

$$u_l(x, y, t) = t \sin(x) \cos(y), \quad (x, y) \in \Omega_l, \quad (4.11)$$

which coincides with the analytical expression of local limit of the nonlocal solution, i.e.,

$$\lim_{\delta \rightarrow 0} u_{nl,\delta}(x, y, t) = u_0(x, y, t) = t \sin(x) \cos(y), \quad (x, y) \in \Omega_{nl}. \quad (4.12)$$

Taking $\Delta t = 10h^2$ and $\delta/h = 3.9$, in the left plot of Figure 10 the amplification factor $\max_i |\lambda_i|$ for the discretized coupling system is plotted versus the Robin coefficient β , for two different spatial discretization length scales $h = 1/10$ and $h = 1/20$. It can be observed that when $h = 1/10$, $\max_i |\lambda_i|$ achieves the minimum when $\beta = 3$; when the spatial discretization size h is decreased to $1/20$, the minimum of $\max_i |\lambda_i|$ occurs at $\beta = 6$. Therefore, the amplification factor analysis suggests $\beta = \frac{3}{10h}$ for this problem setting with spatial discretization length scale h . To verify the analysis of β and investigate the asymptotic compatibility of the coupling framework, in the right plot of Figure 10 we demonstrate the convergence of the numerical solution to the local limit, i.e., to u_0 and u_l , in the L^∞ norm at $T = 1$. Five difference Robin coefficients $\beta = 0, \frac{3}{10h}, \frac{7}{10h}, \frac{10}{h}$ and $\frac{100}{h}$ are considered. We can see that when $\beta = \frac{3}{10h}$, the convergence rate $O(h) = O(\delta)$ is achieved and the numerical solution has the fastest convergence to the local limit. On the other hand, when taking the Neumann-type transmission condition $\beta = 0$, the coupling framework is unstable for small h . This is consistent with the amplification factor analysis on the left plot of Figure 10 where $\max_i |\lambda_i|$ exceeds 1 for $h = 1/20$ and $\beta = 0$. When taking large values of β , the amplification factor $\max_i |\lambda_i|$ gets close to 1, which is also consistent with the slow convergence observed in the $\beta = \frac{100}{h}$ case in the right plot of Figure 10.

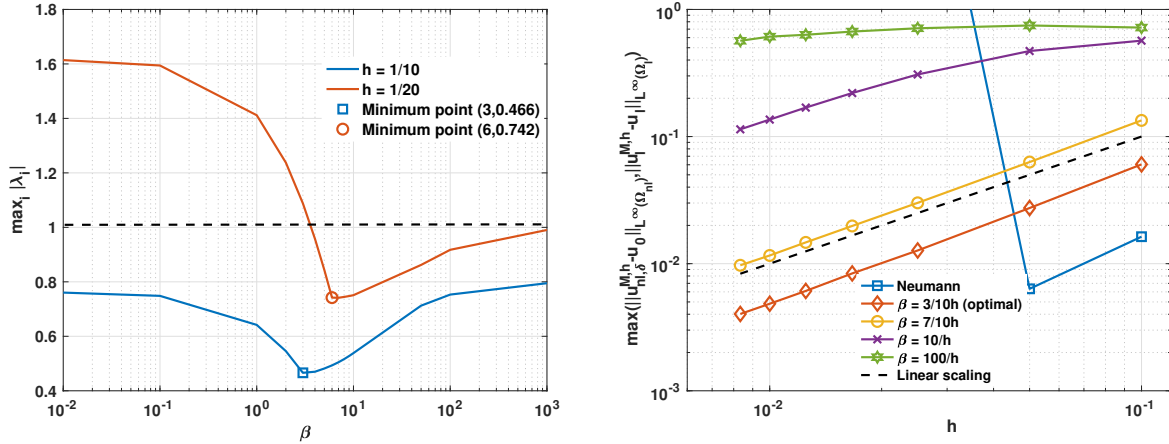


Figure 10: LtN test 1 results for coupling problem with a straight line interface when $\alpha_{nl} = \alpha_l = 1$. Left: the amplification factor $\max_i |\lambda_i|$ as a function of Robin coefficient β , when $h = \{1/10, 1/20\}$. Right: convergence of the numerical solution to the local limit with different Robin coefficients, in the L^∞ norm.

To illustrate the performance of the non-overlapping coupling framework in handling heterogeneous domains with jumps in physical properties, we now consider a coupling problem with different diffusivities in two subdomains. Specifically, we set $\alpha_{nl} = 1$ and $\alpha_l = 2$, and consider two problem settings:

- **Heterogeneous domain setting A:**

$$u^{IC}(x, y) = 0, \text{ for } (x, y) \in \Omega_{nl} \cup \Omega_l,$$

$$u_{nl}^D(x, y, t) = t \sin(x) \cos(y) \text{ for } (x, y) \in B\Omega_d, \quad u_l^D(x, y, t) = t \sin(x) \cos(y), \text{ for } (x, y) \in \Gamma_d,$$

$$f_{nl}(x, y, t) = (1 + 2t) \sin(x) \cos(y), \text{ for } (x, y) \in \Omega_{nl}, \quad f_l(x, y, t) = (1 + 4t) \sin(x) \cos(y), \text{ for } (x, y) \in \Omega_l,$$

$$\lim_{\delta \rightarrow 0} u_{nl,\delta}(x, y, t) = u_0(x, y, t) = t \sin(x) \cos(y) \text{ for } (x, y) \in \Omega_{nl}, \quad u_l(x, y, t) = t \sin(x) \cos(y), \text{ for } (x, y) \in \Omega_l.$$

- **Heterogeneous domain setting B:**

$$u^{IC}(x, y) = 0, \text{ for } (x, y) \in \Omega_{nl} \cup \Omega_l,$$

$$u_{nl}^D(x, y, t) = tx^4 \text{ for } (x, y) \in B\Omega_d, \quad u_l^D(x, y, t) = t(3x^2 - 2x), \text{ for } (x, y) \in \Gamma_d,$$

$$f_{nl}(x, y, t) = x^2(x^2 - 12t), \text{ for } (x, y) \in \Omega_{nl}, \quad f_l(x, y, t) = 3x^2 - 2x - 12t, \text{ for } (x, y) \in \Omega_l,$$

$$\lim_{\delta \rightarrow 0} u_{nl,\delta}(x, y, t) = u_0(x, y, t) = tx^4 \text{ for } (x, y) \in \Omega_{nl}, \quad u_l(x, y, t) = t(3x^2 - 2x), \text{ for } (x, y) \in \Omega_l.$$

In both settings we keep a fixed ratio $\delta/h = 3.9$ and take the time step size $\Delta t = 10h^2$. Note here in setting A, the local limit of $u_{nl,\delta}$ coincides with the analytical local solution u_l , although there is a discontinuity of the external loading across the interface Γ_i . In setting B, besides the discontinuous external loading, when $\delta \rightarrow 0$ the analytical local limit is also not smooth on the interface Γ_i . However, since $u_0 = u_l$ and $\frac{\partial u_0}{\partial \mathbf{n}} = \frac{\partial u_l}{\partial \mathbf{n}}$ on Γ_i , the analytical local limit in setting B still satisfies the classical Dirichlet, Neumann and Robin transmission conditions.

As discussed in Remark 6, since the eigenvalues of Λ depend on Δt , h , Ω_{nl} , Ω_l , α_l and α_{nl} , setting A and setting B should have the same optimal Robin coefficient β , and this optimal β differs from the optimal β we have obtained in the test on homogeneous domain (4.9)-(4.12). In Figure 11, we investigate the optimal Robin coefficient β for heterogeneous domain problem by plotting the amplification factor $\max_i |\lambda_i|$ as a function of β for fixed spatial discretization size $h = 1/10$ and $h = 1/20$. It can be seen that the minimum of $\max_i |\lambda_i|$ occurs at $\beta = \frac{4}{10h}$. To numerically verify the choice of optimal Robin coefficient and to study the asymptotic convergence of the analytical solution, in Figure 12 we demonstrate the convergence results of numerical solution to the analytical local limit at time $T = 1$, for both problem setting A (in the left plot) and problem setting B (in the right plot). Among five different values of Robin coefficient β , it is observed that the optimal convergence $O(h) = O(\delta)$ is achieved at $\beta = \frac{4}{10h}$ – the optimal coefficient suggested in the amplification factor analysis. Slow convergence and divergent results are also observed when taking large β and $\beta = 0$, respectively. This observation is also consistent with the amplification factor analysis in Figure 11, and it further indicates that choosing a proper Robin coefficient is of critical for the numerical stability and the asymptotic convergence rate to the local limit in the proposed coupling framework.

Lastly, we study the patch-test consistency of the proposed local-to-nonlocal coupling framework, by employing fabricated analytical solutions such that the local and nonlocal analytical solutions, u_l and $u_{nl,\delta}$, coincide. In a patch-

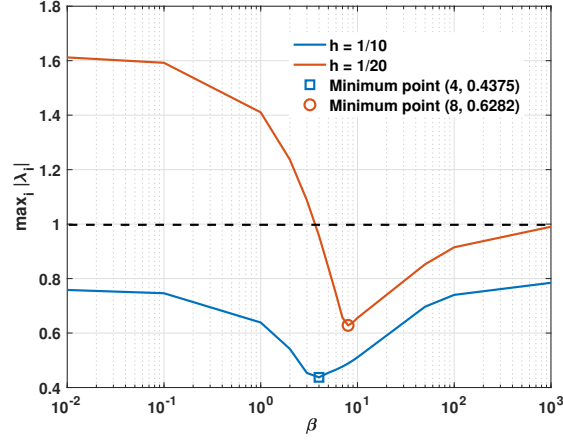


Figure 11: LtN test 1 results with the heterogeneous domain setting ($\alpha_{nl} = 1$, $\alpha_l = 2$): the amplification factor $\max_i |\lambda_i|$ as a function of Robin coefficient β when $h = \{1/10, 1/20\}$.

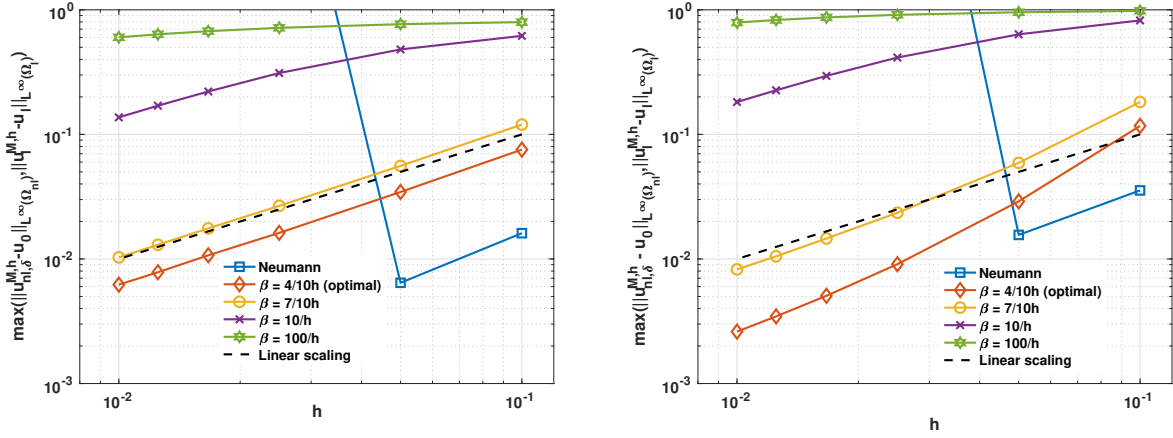


Figure 12: LtN test 1 results for convergence of the numerical solution to the local limit with different Robin coefficients, on heterogeneous domain setting ($\alpha_{nl} = 1$, $\alpha_l = 2$). Left: convergence in the L^∞ norm with problem setting A. Right: convergence in the L^∞ norm with problem setting B.

test consistent coupling framework, the local and nonlocal subproblems by coupling the corresponding models should still return the same problem solution. We first take a linear analytical solution $u_{nl,\delta}(x, y, t) = u_{nl}(x, y, t) = x$ and plot the numerical solution along the middle line $y = 1/2$ in the left plot of Figure 13. In this test we take $\alpha_l = \alpha_{nl} = 1$, $h = 1/20$, $\delta = 3.9h$, $\Delta t = 10h^2 = 1/40$ and the optimal Robin coefficient $\beta = 6$. It is observed that the linear patch test results are in good agreement with the expected linear solution, and the numerical solution is of machine accurate. To further check the quadratic patch test consistency, we take a quadratic analytical solution $u_{nl,\delta}(x, y, t) = u_{nl}(x, y, t) = x^2$ and plot the numerical solution along the middle line $y = 1/2$ in the right plot of Figure 13. Although the numerical solution visually agrees well with the analytical solution, we observe a numerical error since x^2 doesn't belong to the space of piecewise linear finite elements, and therefore the discretization method for the local subproblem introduces a numerical error. In Table 1 we demonstrate the numerical errors in both the L^2 norm and L^∞ norm with different

combinations of h and β . In all tests we take time step $\Delta t = 10h^2$. The results show that the numerical error is almost independent of β and it converges linearly with decreasing h . To further confirms that the numerical error in quadratic patch test is introduced by the linear finite element method, we employ quadratic finite elements for the local subproblem solver and provide the results in Table 2. The numerical results show that the coupling framework achieves machine accuracy. Therefore, when x^2 is in the space of finite elements, the proposed coupling framework passes both linear and quadratic patch tests.

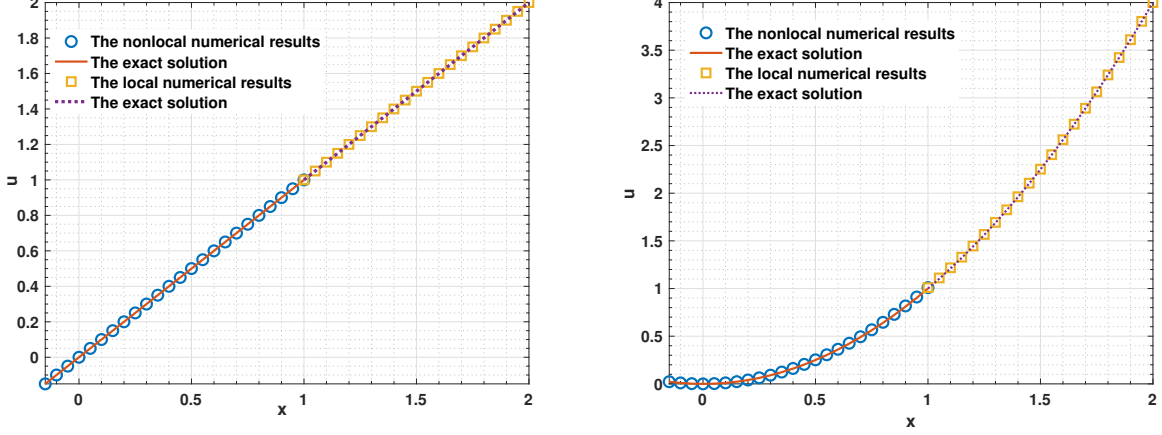


Figure 13: LtN test 1 results for coupling problem with a straight line interface. Left: linear patch test. The comparison of the numerical results with $h = 1/20$, $\beta = 6$ and the analytical solution $u_{nl,\delta} = u_l = x$. Right: quadratic patch test. The comparison of numerical results with $h = 1/20$, $\beta = 6$ and the analytical solution $u_{nl,\delta} = u_l = x^2$.

Local Solver	h	β	Nonlocal problem				Local problem			
			$\ u_{nl} - u^{ex}\ _2$	rate	$\ u_{nl} - u^{ex}\ _\infty$	rate	$\ u_l - u^{ex}\ _2$	rate	$\ u_l - u^{ex}\ _\infty$	rate
linear FEM	1/10	3	6.86×10^{-3}	—	1.98×10^{-2}	—	6.18×10^{-3}	—	1.98×10^{-2}	—
linear FEM	1/20	6	3.17×10^{-3}	1.11	9.72×10^{-3}	1.03	3.00×10^{-3}	1.04	9.72×10^{-3}	1.03
linear FEM	1/40	12	1.50×10^{-3}	1.08	4.75×10^{-3}	1.04	1.46×10^{-3}	1.03	4.75×10^{-3}	1.04
linear FEM	1/80	24	7.28×10^{-4}	1.04	2.34×10^{-3}	1.02	7.19×10^{-4}	1.02	2.34×10^{-3}	1.02
linear FEM	1/10	7	6.74×10^{-3}	—	2.00×10^{-2}	—	6.22×10^{-3}	—	2.00×10^{-2}	—
linear FEM	1/20	14	3.10×10^{-3}	1.12	9.65×10^{-3}	1.05	3.00×10^{-3}	1.05	9.65×10^{-3}	1.05
linear FEM	1/40	28	1.48×10^{-3}	1.07	4.72×10^{-3}	1.03	1.45×10^{-3}	1.05	4.72×10^{-3}	1.03
linear FEM	1/80	56	7.28×10^{-4}	1.02	2.34×10^{-3}	1.01	7.19×10^{-4}	1.04	2.34×10^{-3}	1.01

Table 1: LtN test 1 quadratic patch test results for coupling problem with a straight line interface, using linear finite element method in the local solver. Here $u^{ex} = x^2$ represents the analytical solution.

Local Solver	β	Nonlocal problem				Local problem		
		h_{nl}	$\ u_{nl} - u^{ex}\ _2$	$\ u_{nl} - u^{ex}\ _\infty$	h_l	$\ u_l - u^{ex}\ _2$	$\ u_l - u^{ex}\ _\infty$	
quadratic FEM	6	1/20	6.17×10^{-15}	2.26×10^{-14}	1/10	1.25×10^{-14}	2.31×10^{-14}	
quadratic FEM	12	1/40	1.88×10^{-14}	6.44×10^{-14}	1/20	5.42×10^{-14}	9.59×10^{-14}	

Table 2: LtN test 1 quadratic patch test results for coupling problem with a straight line interface, using quadratic finite element method in the local solver. Here we take $\delta/h_{nl} = 3.0$, and $u^{ex} = x^2$ represents the analytical solution.

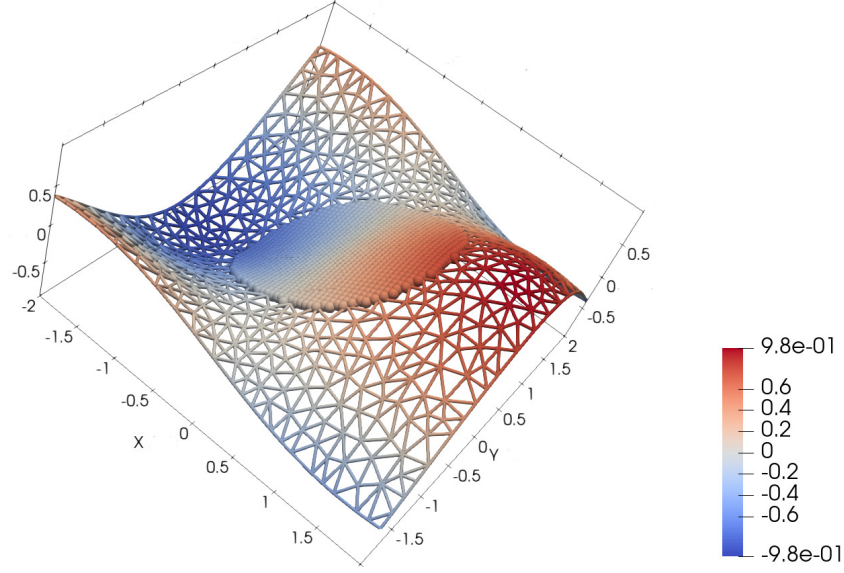


Figure 14: LtN test 2 simulation results for coupling problem with a circular interface when $\alpha_{nl} = \alpha_l = 1$. Here the sphere represents the nonlocal solution with the meshfree solver and the triangular mesh represents the local solution obtained via finite element approximations.

4.3.2. LtN Test 2: coupling problem with a circular interface

We now consider the coupling LtN problem on a circular interface, with the domain settings illustrated in the left side of Figure 5. The nonlocal subdomain is set as a unit circle $\Omega_{nl} = \{(x, y) | x^2 + y^2 \leq 1\}$ and the local subdomain is a 4×4 square region surrounding the unit circle. The local-to-nonlocal interface $\Gamma_i = \{(x, y) | x^2 + y^2 = 1\}$. With this test, we aim to investigate the performance of the proposed coupling framework on local-to-nonlocal coupling problems with curved interfaces. Note that in the finite element solver generated by FEniCS, the circular interface is approximated by a polygon, which introduces an $O(h)$ discretization error in the coupling framework. However, when $\Delta t = O(h^2)$, this discretization error is in the same order as the optimal splitting error $\Delta t/h = O(h)$, so we therefore expect no deterioration on the convergence rate.

We first study the numerical performance when $\alpha_{nl} = \alpha_l = 1$, by employing the same problem setting as in (4.9)-(4.12). Note here since the nonlocal subdomain is fully embedded in the local subdomain, we only need to provide the Dirichlet-type boundary condition on one point for the nonlocal subdomain, to make sure that the nonlocal subproblem is well-defined in the $\beta = 0$ case. Specifically, we set $u_{nl,\delta}(x, y, t) = t \sin(x) \cos(y)$ at $(x, y) = (0, -1)$. The simulation results at $T = 1$ are plotted in Figure 14, where the sphere represents the solution in the nonlocal subdomain and the triangular mesh represents the solution in the local subdomain. To investigate the optimal Robin coefficient, when keeping a fixed ratio $\delta/h = 3.9$ and $\Delta t = 10h^2$ we show the amplification factor $\max_i |\lambda_i|$ from different Robin coefficients in the left plot of Figure 15. In this case, $\max_i |\lambda_i|$ achieves the minimum when $\beta = 0$, which suggests that the Neumann-type transmission condition is the optimal choice. Moreover, we also notice that comparing with the results in test 1, the curves of $\max_i |\lambda_i|$ in test 2 show very different trends. In this case, the value of $\max_i |\lambda_i|$ increases

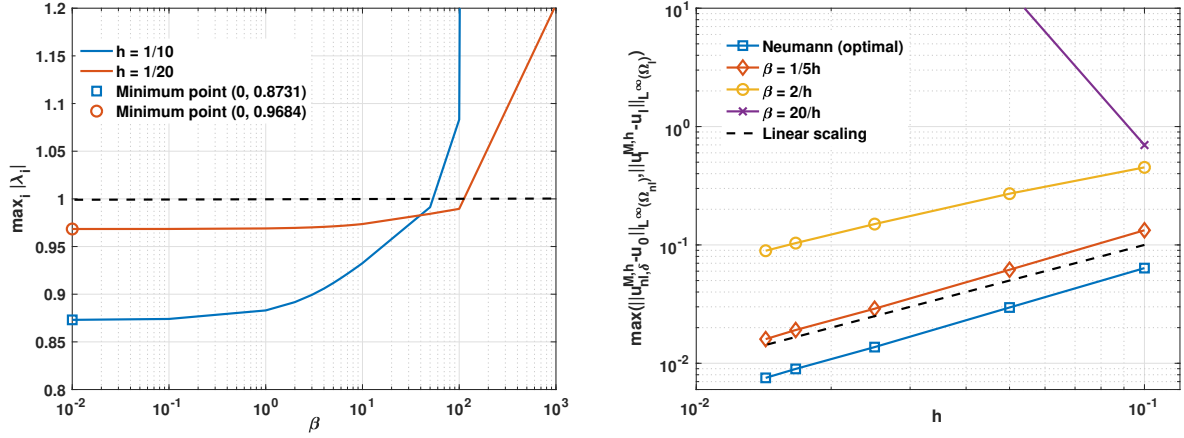


Figure 15: LtN test 2 results for coupling problem with a circular interface when $\alpha_{nl} = \alpha_l = 1$. Left: the amplification factor $\max_i |\lambda_i|$ as a function of Robin coefficient β when $h = \{1/10, 1/20\}$. Right: convergence of the numerical solution to the local limit with respect to different Robin coefficients, in the L^∞ norm.

slowly when $\beta \leq \frac{1}{h}$, and $\max_i |\lambda_i|$ becomes larger than 1 when $\beta \geq \frac{5}{h}$. It indicates that the coupling framework performance should not vary much when employing a small β , and a large β is not a preferable choice for this case since the numerical solution may diverge. To numerically verify the amplification factor analysis and to investigate the asymptotic compatibility of the numerical solution, in the right plot of Figure 15 we show the convergence of the numerical solution to the analytical local limit in the L^∞ norm at time $T = 1$. Among the 4 different Robin coefficients, the case with Neumann-type transmission condition achieves the optimal $O(h)$ convergence to the local limit, and the case with $\beta = \frac{1}{5h}$ also gives a similar convergence rate. When we further increase the Robin coefficient, the convergence rate deteriorates and the coupling framework becomes unstable when $\beta = \frac{20}{h}$. These observations are consistent with the amplification factor analysis. The different trends in Figure 10 and Figure 15 also suggest that the optimal Robin coefficient may vary a lot on different domain settings, and therefore a case-by-case analysis of β is of critical.

On the coupling problem with circular interface, we now investigate the performance of the non-overlapping coupling framework in handling physical property jumps across the interface. In this test we assume that the two subproblems have dramatically different diffusivities $\alpha_{nl} = 1$ and $\alpha_l = 10$, and consider the following two problem settings:

- **Heterogeneous domain setting A:**

$$\begin{aligned}
 u^{IC}(x, y) &= 0, \text{ for } (x, y) \in \Omega_{nl} \cup \Omega_l, \quad u_l^D(x, y, t) = t \sin(x) \cos(y), \text{ for } (x, y) \in \Gamma_d, \\
 f_{nl}(x, y, t) &= (1 + 2t) \sin(x) \cos(y), \text{ for } (x, y) \in \Omega_{nl}, \quad f_l(x, y, t) = (1 + 20t) \sin(x) \cos(y), \text{ for } (x, y) \in \Omega_l, \\
 \lim_{\delta \rightarrow 0} u_{nl, \delta}(x, y, t) &= u_0(x, y, t) = t \sin(x) \cos(y) \text{ for } (x, y) \in \Omega_{nl}, \quad u_l(x, y, t) = t \sin(x) \cos(y), \text{ for } (x, y) \in \Omega_l.
 \end{aligned}$$

- **Heterogeneous domain setting B:**

$$\begin{aligned}
u^{IC}(x, y) &= 0, \text{ for } (x, y) \in \Omega_{nl} \cup \Omega_l, & u_l^D(x, y, t) &= \frac{t((x^2 + y^2)^2 + 1)}{2}, \text{ for } (x, y) \in \Gamma_d, \\
f_{nl}(x, y, t) &= (x^2 + y^2) - 4t, \text{ for } (x, y) \in \Omega_{nl}, & f_l(x, y, t) &= \frac{((x^2 + y^2)^2 + 1)}{2} - 80t(x^2 + y^2), \text{ for } (x, y) \in \Omega_l, \\
\lim_{\delta \rightarrow 0} u_{nl,\delta}(x, y, t) &= u_0(x, y, t) = t(x^2 + y^2) \text{ for } (x, y) \in \Omega_{nl}, & u_l(x, y, t) &= \frac{t((x^2 + y^2)^2 + 1)}{2}, \text{ for } (x, y) \in \Omega_l.
\end{aligned}$$

In both settings we keep a fixed ratio $\delta/h = 3.9$ and take the time step size $\Delta t = 10h^2$. We note that setting A and setting B should have the same optimal Robin coefficient β . To study this optimal Robin coefficient, in Figure 16 we plot the amplification factor $\max_i |\lambda_i|$ as a function of β for fixed spatial discretization sizes $h = 1/10$ and $h = 1/20$, and observe that $\max_i |\lambda_i|$ achieves its minimum at $\beta = 0$, i.e., when the Neumann-type transmission condition is employed. To numerically verify this observation and to study the asymptotic convergence of the analytical solution, in Figure 17 the convergence results of numerical solution to the analytical local limit at time $T = 1$ are plotted versus decreasing h for both problem setting A (in the left plot) and problem setting B (in the right plot). In the case with problem setting A, the fastest convergence $O(h) = O(\delta)$ is achieved when employing the Neumann-type transmission condition. In the case with problem setting B, the results from $\beta = \frac{2}{10h}$ has the smallest difference to the local limit, while tests with $\beta = 0$ and $\beta = \frac{2}{10h}$ achieve almost the same asymptotic convergence rates to the local limit. In both cases, the numerical solution diverges when employing large β , which is consistent with the amplification factor analysis. Therefore, in the test with non-zero interface curvature and heterogeneous diffusivities, the amplification factor analysis also provide a good guidance for the optimal Robin coefficient, and the coupling framework employing optimal Robin coefficient is asymptotically compatible.

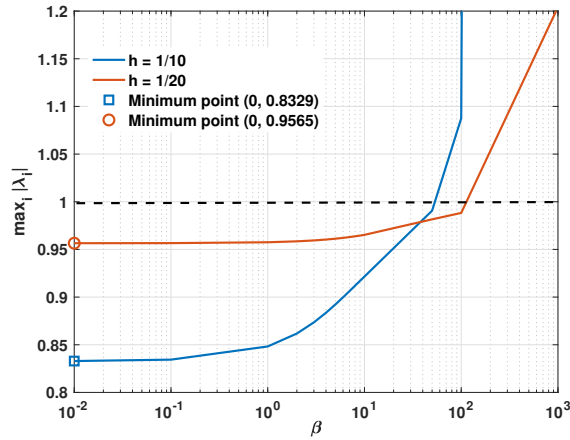


Figure 16: LtN test 2 with the heterogeneous setting ($\alpha_{nl} = 1$, $\alpha_l = 10$): the amplification factor $\max_i |\lambda_i|$ as a function of Robin coefficient β when $h = \{1/10, 1/20\}$.

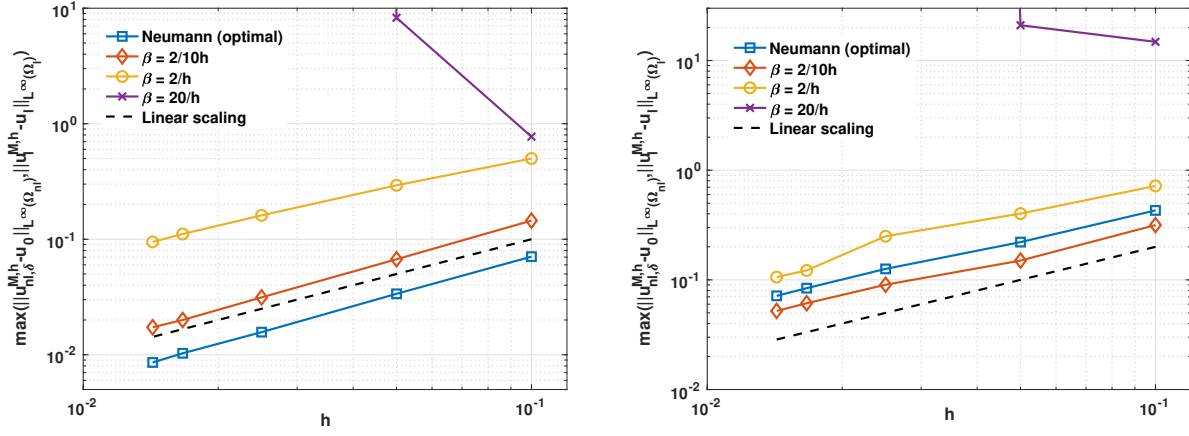


Figure 17: LtN test 2 results for convergence of the numerical solution to the local limit with different Robin coefficients, on heterogeneous domain setting ($\alpha_{nl} = 1$, $\alpha_l = 10$). Left: convergence in the L^∞ norm with problem setting A. Right: convergence in the L^∞ norm with problem setting B.

4.3.3. LtN Test 3: coupling problem with a cross-shape interface

Having demonstrated the asymptotic convergence and the optimal coupling strategy for problems with smooth interfaces, we now apply our approach to a problem with complicated domain settings, as illustrated in the right plot of Figure 5. The nonlocal subdomain is set as a cross-shape region which is not convex, and the local subdomain is a square region surrounding the nonlocal subdomain. With this test, we aim to investigate the performance of the coupling framework on non-trivial domain settings where the coupling interface is non-smooth and includes corners.

We first study the numerical performance when $\alpha_{nl} = \alpha_l = 1$. In this test, the initial temperature $u^I = 0$ in the whole domain. In the nonlocal exterior boundary $B\Omega_d$ and the local exterior boundary Γ_d , we set prescribed Dirichlet boundary conditions as

$$u_{nl}^D(x, y, t) = t^2 \sin(x) \cos(y), \quad u_l^D(x, y, t) = t^2 \sin(x) \cos(y). \quad (4.13)$$

The external loadings are set as

$$f_{nl}(x, y, t) = (2t + 2t^2) \sin(x) \cos(y), \text{ for } (x, y) \in \Omega_{nl}, \quad f_l(x, y, t) = (2t + 2t^2) \sin(x) \cos(y), \text{ for } (x, y) \in \Omega_l. \quad (4.14)$$

This problem has the following analytical limits:

$$\lim_{\delta \rightarrow 0} u_{nl,\delta}(x, y, t) = u_0(x, y, t) = t \sin(x) \cos(y), \quad (x, y) \in \Omega_{nl}, \quad u_l(x, y, t) = t^2 \sin(x) \cos(y), \quad (x, y) \in \Omega_l. \quad (4.15)$$

The simulation results at $T = 1$ are plotted in Figure 18, and the results on amplification factor and convergence to the local limits are demonstrated in Figure 19. In all tests we set $\delta/h = 3.5$ and $\Delta t = 100h^2$. In the left plot of Figure 19 we investigate the optimal Robin coefficient β by plotting $\max_i |\lambda_i|$ as a function of β for two different spatial discretization length scales. It can be observed that the minimum value of $\max_i |\lambda_i|$ occurs at $\beta = \frac{1}{5h}$. Moreover,

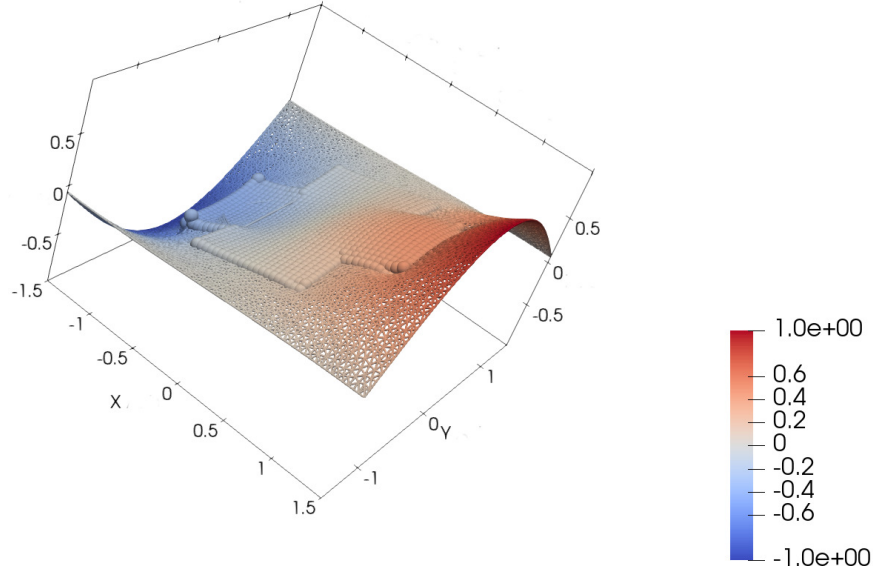


Figure 18: LtN test 3 simulation results for coupling problem with a cross-shape interface when $\alpha_{nl} = \alpha_l = 1$. Here the sphere represents the nonlocal solution with the meshfree solver and the triangular mesh represents the local solution obtained via finite element approximations.

$\max_i |\lambda_i| > 1$ when $\beta = 0$ or $\beta > \frac{10}{h}$, which suggests the possible deteriorating convergence rate or even divergence of the numerical solution. In the right plot of Figure 19, we show the L^∞ norm of the difference between the numerical results and the analytical local limit at time $T = 1$ for four different values of β : 0 , $\frac{1}{5h}$, $\frac{1}{h}$ and $\frac{5}{h}$. The numerical results illustrate that when taking $\beta = 0$, the coupling framework is unstable. Moreover, when employing the optimal Robin coefficient $\beta = \frac{1}{5h}$, the numerical solution has the fastest convergence rate $O(h) = O(\delta)$. Both findings are consistent with the observation from the amplification factor analysis. The above numerical results indicate that the amplification factor analysis helps predicting the optimal Robin coefficient for problems with non-smooth interfaces, and the optimal asymptotic convergence rate $O(h) = O(\delta)$ is achieved.

Lastly, we investigate the performance of the non-overlapping coupling framework in handling heterogeneous domains, by taking $\alpha_{nl} = 1$ and $\alpha_l = 0.1$ and considering the problem setting as follows:

$$\begin{aligned}
 u^{IC}(x, y) &= 0, \text{ for } (x, y) \in \Omega_{nl} \cup \Omega_l, \\
 u_{nl,\delta}^D(x, y, t) &= t^2 \sin(x) \cos(y), \text{ for } (x, y) \in \Gamma_d, \quad u_l^D(x, y, t) = t^2 \sin(x) \cos(y), \text{ for } (x, y) \in \Gamma_d, \\
 f_{nl}(x, y, t) &= 2(t + t^2) \sin(x) \cos(y), \text{ for } (x, y) \in \Omega_{nl}, \quad f_l(x, y, t) = 0.2(t + t^2) \sin(x) \cos(y), \text{ for } (x, y) \in \Omega_l, \\
 \lim_{\delta \rightarrow 0} u_{nl,\delta}(x, y, t) &= u_0(x, y, t) = t^2 \sin(x) \cos(y) \text{ for } (x, y) \in \Omega_{nl}, \quad u_l(x, y, t) = t^2 \sin(x) \cos(y), \text{ for } (x, y) \in \Omega_l.
 \end{aligned}$$

We keep a fixed ratio $\delta/h = 3.5$ and take the time step size $\Delta t = 100h^2$, then investigate the optimal Robin coefficient and the asymptotic convergence performance of the coupling framework. In the left plot of Figure 20, we plot the amplification factor $\max_i |\lambda_i|$ as a function of β for $h = 1/10$ and $h = 1/20$. It is observed that the minimum of

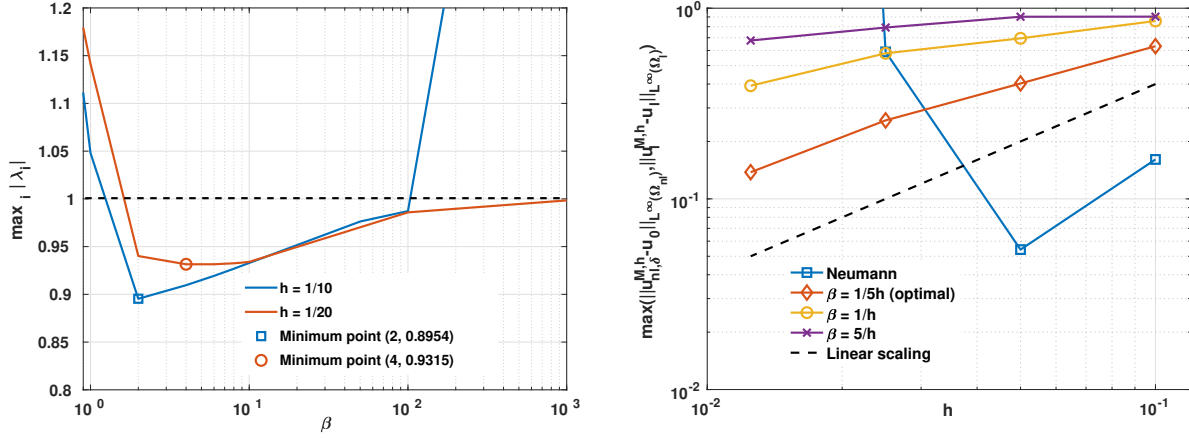


Figure 19: LtN test 3 for the coupling problem with a cross-shape interface when $\alpha_{nl} = \alpha_l = 1$. Left: the amplification factor $\max_i |\lambda_i|$ as a function of Robin coefficient β when $h = \{1/10, 1/20\}$. Right: convergence of the numerical solution to the local limit with different Robin coefficients, in the L^∞ norm.

$\max_i |\lambda_i|$ occurs at $\beta = \frac{1}{5h}$. In the right plot of Figure 20, the convergence of numerical solution to the local limit at $T = 1$ are demonstrated for various values of Robin coefficients: $\beta = 0$, $\frac{1}{5h}$, $\frac{1}{h}$ and $\frac{10}{h}$. Besides verifying the optimal $O(h) = O(\delta)$ convergence rate when taking the optimal Robin coefficient $\beta = \frac{1}{5h}$, the numerical results also demonstrates the importance of picking the optimal β : when taking other values of β , much slower numerical convergence or even divergence are observed.

5. Conclusion

Developing a efficient numerical approach for dynamic local-to-nonlocal (LtN) coupling problem with a non-overlapping domain setting is generally challenging due to both modeling and numerical difficulties. From the modeling aspect, since there is no overlapping region between the two subdomains, the prescription of nonlocal transmission conditions, or volume constraints, becomes non-trivial. From the numerical aspect, when employing the partitioned procedure in LtN coupling problems, one not only has to resolve the numerical stability issue as in the classical domain-decomposition problems, but also has to face the challenge of preserving the asymptotic compatibility.

In this work we have developed an explicit coupling strategy to couple the local and nonlocal heat equations without overlapping regions, based on a new nonlocal Robin-type transmission condition. A meshfree discretization method based on the generalized moving least squares (GMLS) approximation is used to solve for the nonlocal heat equation in the nonlocal subdomain, and a first order finite element method is employed for the classical heat equation in the local subdomain. The coupling framework is based on the partitioned procedure such that the local and nonlocal solvers communicate by exchanging interface conditions, which enables a modular software implementation and the solvers can be treated as black boxes. To resolve the challenge of applying the transmission condition in the nonlocal solver,

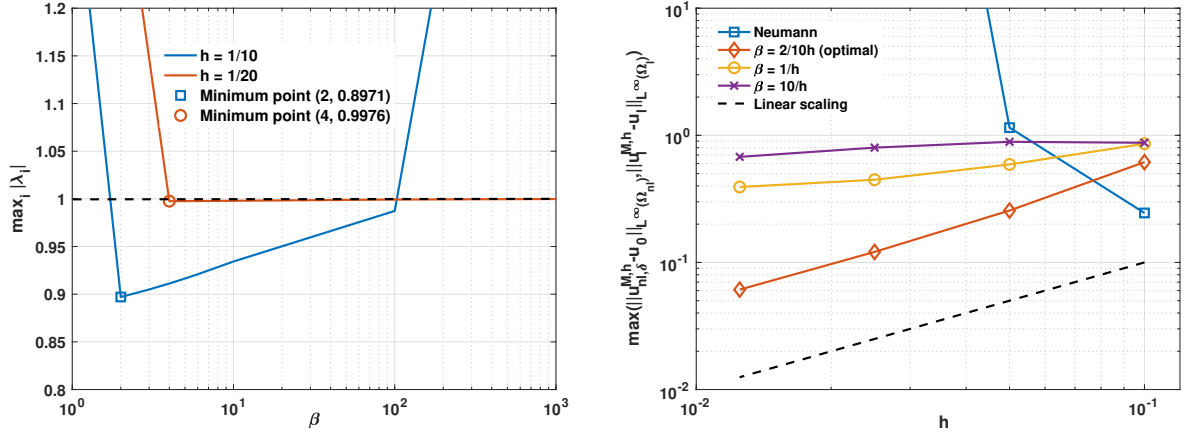


Figure 20: LtN test 3 with the heterogeneous setting ($\alpha_{nl} = 1$, $\alpha_l = 0.1$). Left: the amplification factor $\max_i |\lambda_i|$ as a function of Robin coefficient β when $h = \{1/10, 1/20\}$. Right: convergence of the numerical solution to the local limit with different Robin coefficients, in the L^∞ norm.

we have introduced a new nonlocal Neumann-type constraint for the 2D nonlocal heat equation which is an analogue to the local flux boundary condition. We have theoretically proved that the proposed nonlocal Neumann-type constraint problem converges with the optimal second-order convergence rate $O(\delta^2)$ to the local limit in the $L^\infty(\Omega_{nl})$ norm, and extended this constraint formulation to propose a Robin-type transmission condition. The Neumann and Robin-type formulations are applied on a collar layer inside the domain and therefore require no extrapolation outside the problem domain, which enables the possibility of applying the transmission conditions without overlapping regions. To resolve the numerical challenges in explicit coupling strategy, we provided a numerical approach based on amplification factor analysis to obtain the optimal Robin coefficient. With numerical examples on domains with representative geometries and boundary curvatures, we have verified the robustness and the asymptotic compatibility of both the coupling formulation and the Robin coefficient analysis. Specifically, when employing the optimal Robin coefficient from amplification factor analysis, the optimal L^∞ convergence rate $O(\delta) = O(h)$ to the local limit is observed from the numerical results in all instances.

We note that the formulation described in this paper actually provides an approach for applying the Robin-type boundary condition on general compactly supported nonlocal integro-differential equations (IDEs) with radial kernels. Moreover, the coupling framework provides a general coupling strategy for heterogeneous systems, such as multi-scale and multiphysics problems. As a natural extension, we are working on the development of local-to-nonlocal coupling framework for mechanical problems with multiphysics, such as the coupling approaches for the incompressible peridynamic model and the surrounding fluid, to study the damage induced by variable amplitude environmental loading.

Acknowledgements

H. You and Y. Yu were supported by the National Science Foundation under award DMS 1620434. Y. Yu was also partially supported by the Lehigh faculty research grant. D. Kamensky was supported by start-up funds from the University of California, San Diego.

References

- [1] S. A. Silling, Reformulation of elasticity theory for discontinuities and long-range forces, *Journal of the Mechanics and Physics of Solids* 48 (1) (2000) 175–209.
- [2] Z. P. Bažant, M. Jirásek, Nonlocal integral formulations of plasticity and damage: survey of progress, *Journal of Engineering Mechanics* 128 (11) (2002) 1119–1149.
- [3] M. Zimmermann, A continuum theory with long-range forces for solids, Ph.D. thesis, Massachusetts Institute of Technology (2005).
- [4] E. Emmrich, O. Weckner, Analysis and numerical approximation of an integro-differential equation modeling non-local effects in linear elasticity, *Mathematics and Mechanics of Solids* 12 (4) (2007) 363–384.
- [5] E. Emmrich, O. Weckner, et al., On the well-posedness of the linear peridynamic model and its convergence towards the navier equation of linear elasticity, *Communications in Mathematical Sciences* 5 (4) (2007) 851–864.
- [6] K. Zhou, Q. Du, Mathematical and numerical analysis of linear peridynamic models with nonlocal boundary conditions, *SIAM Journal on Numerical Analysis* 48 (5) (2010) 1759–1780.
- [7] Q. Du, K. Zhou, Mathematical analysis for the peridynamic nonlocal continuum theory, *ESAIM: Mathematical Modelling and Numerical Analysis* 45 (02) (2011) 217–234.
- [8] I. Podlubny, Fractional differential equations: an introduction to fractional derivatives, fractional differential equations, to methods of their solution and some of their applications, Vol. 198, Academic Press, 1998.
- [9] F. Mainardi, Fractional calculus and waves in linear viscoelasticity: an introduction to mathematical models, World Scientific, 2010.
- [10] R. L. Magin, Fractional calculus in bioengineering, Begell House Publishers Inc., Redding, CT, 2006.
- [11] N. Burch, R. Lehoucq, Classical, nonlocal, and fractional diffusion equations on bounded domains, *International Journal for Multiscale Computational Engineering* 9 (6).

- [12] Q. Du, Z. Huang, R. B. Lehoucq, Nonlocal convection-diffusion volume-constrained problems and jump processes., *Discrete & Continuous Dynamical Systems-Series B* 19 (4).
- [13] O. Defterli, M. D’Elia, Q. Du, M. Gunzburger, R. Lehoucq, M. M. Meerschaert, Fractional diffusion on bounded domains, *Fractional Calculus and Applied Analysis* 18 (2) (2015) 342–360.
- [14] A. Lischke, G. Pang, M. Gulian, F. Song, C. Glusa, X. Zheng, Z. Mao, W. Cai, M. M. Meerschaert, M. Ainsworth, et al., What is the fractional laplacian?, *arXiv preprint arXiv:1801.09767*.
- [15] Q. Du, R. Lipton, Peridynamics, fracture, and nonlocal continuum models, *SIAM News* 47 (3).
- [16] X. Antoine, H. Barucq, Approximation by generalized impedance boundary conditions of a transmission problem in acoustic scattering, *ESAIM: Mathematical Modelling and Numerical Analysis* 39 (5) (2005) 1041–1059.
- [17] K. Dayal, K. Bhattacharya, A real-space non-local phase-field model of ferroelectric domain patterns in complex geometries, *Acta Materialia* 55 (6) (2007) 1907–1917.
- [18] E. W. Sachs, M. Schu, A priori error estimates for reduced order models in finance, *ESAIM: Mathematical Modelling and Numerical Analysis* 47 (2) (2013) 449–469.
- [19] C. Bucur, E. Valdinoci, *Nonlocal diffusion and applications*, Vol. 20, Springer, 2016.
- [20] P. Seleson, M. Gunzburger, M. L. Parks, Interface problems in nonlocal diffusion and sharp transitions between local and nonlocal domains, *Computer Methods in Applied Mechanics and Engineering* 266 (2013) 185–204.
- [21] Y. Azdoud, F. Han, G. Lubineau, A morphing framework to couple non-local and local anisotropic continua, *International Journal of Solids and Structures* 50 (9) (2013) 1332–1341.
- [22] F. Han, G. Lubineau, Coupling of nonlocal and local continuum models by the arlequin approach, *International Journal for Numerical Methods in Engineering* 89 (6) (2012) 671–685.
- [23] S. Prudhomme, H. B. Dhia, P. T. Bauman, N. Elkhodja, J. T. Oden, Computational analysis of modeling error for the coupling of particle and continuum models by the arlequin method, *Computer Methods in Applied Mechanics and Engineering* 197 (41) (2008) 3399–3409.
- [24] M. D’Elia, M. Gunzburger, Optimal distributed control of nonlocal steady diffusion problems, *SIAM Journal on Control and Optimization* 52 (1) (2014) 243–273.
- [25] Q. Du, X. H. Li, J. Lu, X. Tian, A quasinonlocal coupling method for nonlocal and local diffusion models, *arXiv preprint arXiv:1704.00348*.
- [26] X. H. Li, J. Lu, Quasinonlocal coupling of nonlocal diffusions, *SIAM Journal on Numerical Analysis* 55 (2017) 2394–2415.

- [27] M. D'Elia, M. Perego, P. Bochev, D. Littlewood, A coupling strategy for nonlocal and local diffusion models with mixed volume constraints and boundary conditions, *Computers & Mathematics with Applications* 71 (11) (2016) 2218–2230.
- [28] G. Lubineau, Y. Azdoud, F. Han, C. Rey, A. Askari, A morphing strategy to couple non-local to local continuum mechanics, *Journal of the Mechanics and Physics of Solids* 60 (6) (2012) 1088–1102.
- [29] P. Seleson, Y. D. Ha, S. Beneddine, Concurrent coupling of bond-based peridynamics and the navier equation of classical elasticity by blending, *Journal for Multiscale Computational Engineering* 13 (2) (2015) 91–113.
- [30] E. Askari, F. Bobaru, R. Lehoucq, M. Parks, S. Silling, O. Weckner, Peridynamics for multiscale materials modeling, in: *Journal of Physics: Conference Series*, Vol. 125, IOP Publishing, 2008, p. 012078.
- [31] Y. Tao, X. Tian, Q. Du, Nonlocal models with heterogeneous localization and their application to seamless local-nonlocal coupling, *Multiscale Modeling & Simulation* 17 (3) (2019) 1052–1075.
- [32] S. Silling, D. Littlewood, P. Seleson, Variable horizon in a peridynamic medium, *Journal of Mechanics of Materials and Structures* 10 (5) (2015) 591–612.
- [33] R. W. Macek, S. A. Silling, Peridynamics via finite element analysis, *Finite Elements in Analysis and Design* 43 (15) (2007) 1169 – 1178.
- [34] E. Oterkus, Peridynamic theory for modeling three-dimensional damage growth in metallic and composite structures, Ph.D. thesis, The University of Arizona (2010).
- [35] A. Agwai, I. Guven, E. Madenci, Damage prediction for electronic package drop test using finite element method and peridynamic theory, in: *Electronic Components and Technology Conference, 2009. ECTC 2009. 59th, 2009*, pp. 565–569.
- [36] W. Liu, J. W. Hong, A coupling approach of discretized peridynamics with finite element method, *Computer Methods in Applied Mechanics and Engineering* 15 (2012) 163 – 175.
- [37] J. Lee, S. E. Oh, J.-W. Hong, Parallel programming of a peridynamics code coupled with finite element method, *International Journal of Fracture* (2016) 1–16doi:10.1007/s10704-016-0121-y.
URL <http://dx.doi.org/10.1007/s10704-016-0121-y>
- [38] F. Han, G. Lubineau, Y. Azdoud, A. Askari, A morphing approach to couple state-based peridynamics with classical continuum mechanics, *Computer Methods in Applied Mechanics and Engineering* 301 (2016) 336 – 358. doi:<http://dx.doi.org/10.1016/j.cma.2015.12.024>.
URL <http://www.sciencedirect.com/science/article/pii/S0045782515004302>

- [39] U. Galvanetto, T. Mudric, A. Shojaei, M. Zaccariotto, An effective way to couple {FEM} meshes and peridynamics grids for the solution of static equilibrium problems, *Mechanics Research Communications* 76 (2016) 41 – 47. doi:<http://dx.doi.org/10.1016/j.mechrescom.2016.06.006>.
URL <http://www.sciencedirect.com/science/article/pii/S0093641316300611>
- [40] Y. Yu, F. F. Bargas, H. You, M. L. Parks, M. L. Bittencourt, G. E. Karniadakis, A partitioned coupling framework for peridynamics and classical theory: Analysis and simulations, *Computer Methods in Applied Mechanics and Engineering* 340 (2018) 905–931.
- [41] Q. Du, X. H. Li, J. Lu, X. Tian, A quasi-nonlocal coupling method for nonlocal and local diffusion models, *SIAM Journal on Numerical Analysis* 56 (2018) 1386–1404.
- [42] P. Seleson, S. Beneddine, S. Prudhomme, A force-based coupling scheme for peridynamics and classical elasticity, *Computational Materials Science* 66 (2013) 34–49.
- [43] F. Bobaru, Y. D. Ha, Adaptive refinement and multiscale modeling in 2D peridynamics, *International Journal for Multiscale Computational Engineering* 9 (6).
- [44] F. Bobaru, M. Yang, L. F. Alves, S. A. Silling, E. Askari, J. Xu, Convergence, adaptive refinement, and scaling in 1d peridynamics, *International Journal for Numerical Methods in Engineering* 77 (6) (2009) 852–877.
- [45] H. Ren, X. Zhuang, Y. Cai, T. Rabczuk, Dual-horizon peridynamics, *International Journal for Numerical Methods in Engineering* 108 (12) (2016) 1451–1476.
- [46] P. D. Seleson, Peridynamic multiscale models for the mechanics of materials: constitutive relations, upscaling from atomistic systems, and interface problems, The Florida State University.
- [47] X. Tian, Q. Du, Trace theorems for some nonlocal function spaces with heterogeneous localization, *SIAM Journal on Mathematical Analysis* 49 (2) (2017) 1621–1644.
- [48] X. Tian, Q. Du, Asymptotically compatible schemes and applications to robust discretization of nonlocal models, *SIAM Journal on Numerical Analysis* 52 (4) (2014) 1641–1665.
- [49] Y. Tao, X. Tian, Q. Du, Nonlocal diffusion and peridynamic models with Neumann type constraints and their numerical approximations, *Applied Mathematics and Computation* 305 (2017) 282–298.
- [50] M. D’Elia, D. Littlewood, P. Bochev, M. Perego, An optimization-based coupling strategy for local and nonlocal elasticity problems, 2018, presented at the 13th World Congress on Computational Mechanics (WCCM XIII), July 2018, New York, NY, USA.
- [51] Q. Du, J. Zhang, C. Zheng, On uniform second order nonlocal approximations to linear two-point boundary value problems.

- [52] C. Cortazar, M. Elgueta, J. D. Rossi, N. Wolanski, Boundary fluxes for nonlocal diffusion, *Journal of Differential Equations* 234 (2) (2007) 360–390.
- [53] C. Cortazar, M. Elgueta, J. D. Rossi, N. Wolanski, How to approximate the heat equation with Neumann boundary conditions by nonlocal diffusion problems, *Archive for Rational Mechanics and Analysis* 187 (1) (2008) 137–156.
- [54] M. D’Elia, X. Tian, Y. Yu, A physically-consistent, flexible and efficient strategy to convert local boundary conditions into nonlocal volume constraints, *arXiv preprint arXiv:1906.04259*.
- [55] N. Trask, H. You, Y. Yu, M. L. Parks, An asymptotically compatible meshfree quadrature rule for nonlocal problems with applications to peridynamics, *Computer Methods in Applied Mechanics and Engineering* 343 (2019) 151–165.
- [56] H. You, X.-Y. Lu, N. Trask, Y. Yu, An asymptotically compatible approach for Neumann-type boundary condition on nonlocal problems, *Under revision*.
- [57] S. Badia, F. Nobile, C. Vergara, Fluid-structure partitioned procedures based on Robin transmission conditions, *Journal of Computational Physics* 227 (14) (2008) 7027–7051.
- [58] W. Chen, M. Gunzburger, F. Hua, X. Wang, A parallel Robin-Robin domain decomposition method for the Stokes-Darcy system, *SIAM Journal on Numerical Analysis* 49 (3) (2011) 1064–1084.
- [59] M. Discacciati, A. Quarteroni, A. Valli, Robin-Robin domain decomposition methods for the Stokes-Darcy coupling, *SIAM Journal on Numerical Analysis* 45 (3) (2007) 1246–1268.
- [60] J. Douglas, C.-S. Huang, An accelerated domain decomposition procedure based on Robin transmission conditions, *BIT Numerical Mathematics* 37 (3) (1997) 678–686.
- [61] H. Wendland, *Scattered data approximation*, Vol. 17, Cambridge university press, 2004.
- [62] M. Alnæs, J. Blechta, J. Hake, A. Johansson, B. Kehlet, A. Logg, C. Richardson, J. Ring, M. E. Rognes, G. N. Wells, The FEniCS project version 1.5, *Archive of Numerical Software* 3 (100).
- [63] A. Logg, K.-A. Mardal, G. Wells, *Automated solution of differential equations by the finite element method: The FEniCS book*, Vol. 84, Springer Science & Business Media, 2012.
- [64] H. S. Park, P. A. Klein, G. J. Wagner, A surface cauchy–born model for nanoscale materials, *International Journal for Numerical Methods in Engineering* 68 (10) (2006) 1072–1095.
- [65] A. C. Ponce, An estimate in the spirit of poincaré’s inequality, *Journal of the European Mathematical Society* 6 (1) (2004) 1–15.

- [66] Q. Du, M. Gunzburger, R. B. Lehoucq, K. Zhou, Analysis and approximation of nonlocal diffusion problems with volume constraints, *SIAM review* 54 (4) (2012) 667–696.
- [67] T. Mengesha, Q. Du, Analysis of a scalar peridynamic model with a sign changing kernel, *Disc. Cont. Dyn. Sys. B* 18 (2013) 1415–1437.
- [68] N. V. Krylov, *Lectures on elliptic and parabolic equations in Holder spaces*, no. 12, American Mathematical Soc., 1996.
- [69] M. Hillman, M. Pasetto, G. Zhou, Generalized reproducing kernel peridynamics: unification of local and non-local meshfree methods, non-local derivative operations, and an arbitrary-order state-based peridynamic formulation, *Computational Particle Mechanics*.
- [70] J. Degroote, K.-J. Bathe, J. Vierendeels, Performance of a new partitioned procedure versus a monolithic procedure in fluid–structure interaction, *Computers & Structures* 87 (11-12) (2009) 793–801.
- [71] A. Quarteroni, A. Valli, *Domain decomposition methods for partial differential equations*, no. BOOK, Oxford University Press, 1999.
- [72] T. Mathew, *Domain decomposition methods for the numerical solution of partial differential equations*, Vol. 61, Springer Science & Business Media, 2008.
- [73] A. Toselli, O. Widlund, *Domain decomposition methods-algorithms and theory*, Vol. 34, Springer Science & Business Media, 2006.
- [74] E. Burman, M. A. Fernández, Explicit strategies for incompressible fluid-structure interaction problems: Nitsche type mortaring versus Robin–Robin coupling, *International Journal for Numerical Methods in Engineering* 97 (10) (2014) 739–758.
- [75] M. A. Fernández, J. Mullaert, M. Vidrascu, Generalized Robin–Neumann explicit coupling schemes for incompressible fluid-structure interaction: Stability analysis and numerics, *International Journal for Numerical Methods in Engineering* 101 (3) (2015) 199–229.
- [76] D. Levin, The approximation power of moving least-squares, *Mathematics of computation* 67 (224) (1998) 1517–1531.
- [77] E. Burman, R. Durst, J. Guzman, Stability and error analysis of a splitting method using Robin-Robin coupling applied to a fluid-structure interaction problem, *arXiv preprint arXiv:1911.06760*.